UNIVERSITY POLITEHNICA OF BUCHAREST

Faculty of Biotechnical Systems Engineering

Mechanical Engineering Department

PHD THESIS SUMMARY

Dynamics of Rotating Machinery in Non-inertial Frames

Dinamica Maşinilor Rotative în Sisteme Neinerţiale

SCIENTIFIC COORDINATOR:

Prof. PhD.
Ion STROE

AUTHOR:

Rs. Eng.
Cristian Mihail STĂNICĂ

Bucharest, 2020

CONTENTS

KEY WORDS

Rotor, rotordynamics, non-inertial, frame, vibration, frequency response, finite element.

INTRODUCTION

Virtually all man-made machines used in the field of transport have units and motors based on the action of rotor assemblies. Safety constraints in the operation of vehicles require the development of calculation methods at supercritical speeds and in non-inertial systems.

The failure of the rotor components must be evaluated in order to allow the vehicle to be stopped safely. Thus, in areas such as aeronautics, in order to accept an in-flight propulsion system, it is necessary to successfully perform tests that involve failure during operation of the rotor assembly.

For all the situations described above, calculation methods appropriate to the particularities of each analyzed situation are currently being developed.

The starting point of the calculation method is the Lagrange equation of motion. It was used by the first theorists Voinea R. and Stroe I. [1] to describe the dynamics of rotors in a non-inertial reference system. Then later, in the development of the finite element theory by Arne Vollan and Louis Komzsik in the paper [2] the complete form of the Lagrange equation of motion was approached considering also the terms corresponding to the dissipative energy.

CHAPTER 1

STATE OF THE ART

1.1 GENERAL DESCRIPTION OF THE ROTORDYNAMICS DOMAIN

Towards the end of the 19th century, Rankine made the first theoretical development of rotor dynamics based on the need to design steam turbines and highlighted the existence of the first critical speed for all rotors. Due to the fact that the existing imbalance in the rotor is considered to generate a centrifugal force proportional to the rotational speed (and above the first critical speed) it was incorrectly recommended that all rotors be designed with the operating range below the first critical speed.

Later DeLaval and Osborne Reynolds make important experimental contributions that allow Jeffcott in 1919 to develop the first correct theoretical model of rotor dynamics with the correct representation of phenomena occurring at supercritical speeds. [3] The series of surprises continues with the discovery of Kimball, A. L. about the role of internal damping of the rotor on the unstable operation [4] of rotors at supercritical speeds. This contradicts the intuition that damping always leads to the attenuation of vibrations and cannot even be the source of these vibrations. The advent of high-speed rotary machines in twentieth-century aerospace applications led to the discovery of additional effects in seals, the Lomakin effect [5] and for the interaction of rotors with the surrounding fluid, Alford force. [6]

At international level, in 1992 a decisive step was taken regarding the dynamics of rotary machines by the publication by Voinea R. and Stroe I. of the calculation methodology in non-inertial reference system [1], a methodology that is still used today and which makes the object of the detailed development in the present thesis. This methodology remains to date the most general and comprehensive theoretical approach to non-inertiality in the field of rotary machines. At the national level, the concern in this direction is continued by Stroe I. highlighted in the paper [7] with a strong applicative character on the protection of high value industrial installations such as high power turbines from the effects of earthquakes. From the point of view of the finite element method, the most comprehensive approach to the subject of non-inertial reference rotary machines is currently made by Vollan A. in the book "Computational Techniques of Rotor Dynamics with the Finite Element Method" [2]. If Friswell [8] devotes a chapter to this non-inertial approach, Vollan bases his entire theory, his entire book, on the principle of non-inertiality.

1.2 THE MOVEMENT OF THE MATERIAL POINT IN A NON-INERTIAL REFERENCE SYSTEM WITH A FIX AXIS REGARDING AN INERTIAL REFERENCE SYSTEM

In order to understand the principles that govern the operation of rotary machines, the second law of motion published by Newton is used as a foundation. This principle states that, in an inertial reference system, the sum of all forces acting on a physical object is equal to the product of the mass of that object and its acceleration.

$$\{F\} = m \cdot \{a\} \tag{1.1}$$

Rotors are usually designed and analyzed in the non-inertial reference system linked to the rotor so that its components can be analyzed using the usual techniques of classical theory. In this sense, the second principle of dynamics stated by Newton is adapted to understand the phenomena that occur in the case of a non-inertial reference system characterized by a rotational speed defined by the vector {Ω} [rad/sec].

$$m\left(\frac{d^2\{r\}}{dt^2}\right)_{inert} + \left[-m\left(\frac{d^2\{r\}}{dt^2}\right) - m\cdot 2\cdot\{\Omega\}\times\left(\frac{d\{r\}}{dt}\right) - m\cdot\{\Omega\}\times\left(\{\Omega\}\times\{r\}\right) - m\cdot\frac{d\{\Omega\}}{dt}\times\{r\}\right]_{rot} = 0. \tag{1.2}$$

From the form deduced above it follows that the trajectory of a material point of mass m in the non-inertially rotating reference system can be determined by adding to Newton's second law three fictitious forces: centrifugal force, Coriolis force and transport force.

$$\text{centrifugal force} = -m\cdot\{\Omega\}\times\left(\{\Omega\}\times\{r\}\right) \tag{1.3}$$

$$\text{Coriolis force} = -m \cdot 2 \cdot \{\Omega\} \times \left(\frac{d\{r\}}{dt} \right)_{rot} \tag{1.4}$$

$$\text{transport force} = -m \cdot \frac{d\{\Omega\}}{dt} \times \{r\} \tag{1.5}$$

1.3 TRANSLATION MOTIONS OF A RIGID SOLID MODELED AS A DISK IN A NON-INERTIAL REFERENCE SYSTEM SUBJECTED TO ROTATIONS

The starting point in the physical substantiation of computational methods in non-inertial reference systems is the Lagrange equation of motion. In this thesis the theory developed by Voinea R. and Stroe I. [1] is used in order to be applied to the finite elements method. Unlike most works in the field of rotary machines in this chapter it will be considered that the analyzed rotor describes not only a rotational movement in relation to an inertial reference system but also a variable translational movement.

In this method, the rotor disk is considered rigid and concentrating the entire mass of the rotor and the shaft flexible and without mass. In the following chapters and paragraphs, the paper [9] published by the author in order to support this thesis will be developed in more detail.

In the figure below one can see the three coordinate systems used to formulate the Lagrange equations and then the equations of motion for the studied rotor.

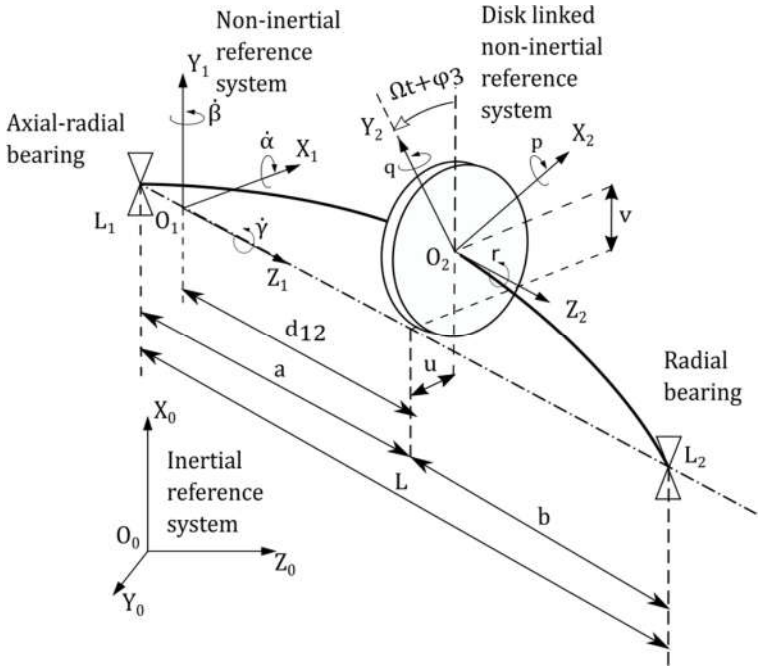

Figure 1.1. Rotor in a non-inertial reference system.

Using XYZ type Euler transformation with angles $\varphi_1, \varphi_2, \Phi_3$ ($s_{1,2} = \sin\varphi_{1,2}$, $c_{1,2} = \cos\varphi_{1,2}$...) for the disk linked reference system, the rotational speed of the disk regarding the inertial system (expressed in the disk linked non-inertial system) is

$$\bar{\omega}_{20} = \begin{Bmatrix} p \\ q \\ r \end{Bmatrix} = \bar{\omega}_{2\,Euler} + \bar{\omega}_{12} = \begin{bmatrix} c_2c_3 & s_3 & 0 \\ -c_2s_3 & c_3 & 0 \\ s_2 & 0 & 1 \end{bmatrix} \cdot \begin{Bmatrix} \dot{\varphi}_1 \\ \dot{\varphi}_2 \\ \dot{\Phi}_3 \end{Bmatrix} + T_{2-1} \begin{Bmatrix} \dot{\alpha} \\ \dot{\beta} \\ \dot{\gamma} \end{Bmatrix}. \tag{1.6}$$

After performing the multiplication and addition results

$$\begin{Bmatrix} p \\ q \\ r \end{Bmatrix} = \begin{Bmatrix} s_3(\dot{\varphi}_2 + \dot{\gamma}s_1 + \dot{\beta}c_1) + c_3(s_2(\dot{\beta}s_1 + \dot{\gamma}c_1) + c_2(\dot{\varphi}_1 + \dot{\alpha})) \\ s_3(s_2(c_1\dot{\gamma} - s_1\dot{\beta}) - c_2(\dot{\varphi}_1 + \dot{\alpha})) + c_3(\dot{\gamma}s_1 + \dot{\beta}c_1 + \dot{\varphi}_2) \\ s_2(\dot{\varphi}_1 + \dot{\alpha}) + c_2(\dot{\gamma}c_1 - \dot{\beta}s_1) + \dot{\Phi}_3 \end{Bmatrix} \tag{1.7}$$

To find out the speed of translation of the center of mass for the rotor disk, one can observe that the origin of the reference system $O_2X_2Y_2Z_2$ is exactly in the center of mass of the disk. Thus, noting with index d the speed of the disk and with index 0,1,2 the variables associated with the three reference systems, the translation speed of the disk is obtained,

$$\bar{v}_{d0} = \bar{v}_{20} = \bar{v}_{21} + \bar{v}_{10} + \bar{\omega}_{10} \times \overline{O_1O_2}. \tag{1.8}$$

Considering the distance between the origins O_1 and O_2 as d_{12}, using the notation u, v, w for the displacements of the center of mass of the disk in the reference system $O_1X_1Y_1Z_1$ then it results

$$\begin{Bmatrix} v_{xd0} \\ v_{yd0} \\ v_{zd0} \end{Bmatrix} = \begin{Bmatrix} \dot{u}_d \\ \dot{v}_d \\ \dot{w}_d \end{Bmatrix} + \begin{Bmatrix} v_{x10} \\ v_{y10} \\ v_{z10} \end{Bmatrix} + \underbrace{\begin{bmatrix} 0 & -\dot{\gamma} & \dot{\beta} \\ \dot{\gamma} & 0 & -\dot{\alpha} \\ -\dot{\beta} & \dot{\alpha} & 0 \end{bmatrix} \begin{Bmatrix} u_d \\ v_d \\ d_{12} + w_d \end{Bmatrix}}_{\text{viteza de transport}}. \tag{1.9}$$

After performing the multiplication and addition of the matrices it results

$$\begin{Bmatrix} v_{xd0} \\ v_{yd0} \\ v_{zd0} \end{Bmatrix} = \begin{Bmatrix} \dot{u}_d + v_{x10} + \dot{\beta}(d_{12} + w_d) - \dot{\gamma}v_d \\ \dot{v}_d + v_{y10} + \dot{\gamma}u_d - \dot{\alpha}(d_{12} + w_d) \\ \dot{w}_d + v_{z10} + \dot{\alpha}v_d - \dot{\beta}u_d \end{Bmatrix} \tag{1.10}$$

In the above system of equations, because w_d and $\dot{w}_d$ are much smaller relative to u_d, v_d, $\dot{u}_d$ and $\dot{v}_d$, they can be neglected in the final stage of calculating the lateral vibrations of the rotary machine shaft.

CHAPTER 2

THE EQUATION OF MOTION IN A NON-INERTIAL REFERENCE SYSTEM

1 2.1 THE EQUATION OF MOTION OF THE RIGID SOLID IN A NON-INERTIAL REFERENCE SYSTEM

Considering the expressions of velocities and forces deduced in previous chapters, Lagrange equations can be formulated. For this purpose, the Lagrangian corresponding to the application is first determined.

$$L = E - V. \tag{2.1}$$

With E is denoted the kinetic energy which is in turn made up of the kinetic energy of translation E_t and the kinetic energy of rotation. E_r. With V is noted the potential energy.

$$E = E_t + E_r, \quad E = \frac{m_d}{2}\left(v_{xd0}^2 + v_{yd0}^2 + v_{zd0}^2\right) + \frac{1}{2}\left[I_d\left(p^2 + q^2\right) + I_p r^2\right]. \tag{2.2}$$

The kinetic energy is determined considering the relations (1.7) and (1.10) in the above equation. (where p, q, r are the components of the angular speed ω_{20} defined in (1.6))

The potential energy using the terms from, (2.23).

$$\begin{aligned} V = {} & \frac{k_{tor}\varphi_3{}^2}{2} + \frac{k_{44}\left(\varphi_2{}^2 + \varphi_1{}^2\right)}{2} + k_{14}\left(u\varphi_2 - v\varphi_1\right) + \frac{k_{ax}w^2}{2} + \frac{k_{11}\left(v^2 + u^2\right)}{2} - \\ & + \frac{F_{ax}}{2\cdot a}\left(u^2 + v^2\right) + \frac{F_{ax}\cdot a}{2\cdot 5{,}844}\left(\varphi_1^2 + \varphi_2^2\right)\cdot \qquad \left(F_{ax} = \frac{E\cdot A}{a}\cdot w\right) \end{aligned} \tag{2.3}$$

Combining the equations (2.1), (2.2) and (2.3) with Lagrange equations

$$\frac{d}{dt}\left(\frac{\partial L}{\partial \dot{q}_k}\right) - \frac{\partial L}{\partial q_k} = 0, \quad \text{(k=1, 2, 3, 4)} \tag{2.4}$$

a system of linear equations is obtained according to the generalized coordinates that can be solved by relatively fast classical methods such as the eigenvalues method if the small terms are approximated with linear terms and the small terms of higher order are neglected.

Then organizing them in matrix form results the equation of motion. After making derivations in (2.4) and using the approximations of the small terms results

$$\begin{aligned} & \ddot{u}\cdot m_d - 2\cdot m_d\cdot\dot{\gamma}\cdot\dot{v} + u\cdot\left(-\dot{\gamma}^2 m_d - \dot{\beta}^2 m_d + k_{11} + \frac{F_{ax}}{a}\right) + v\cdot\left(\dot{\alpha}\cdot\dot{\beta}\cdot m_d\right) + \varphi_2\cdot k_{14} + \\ & \qquad + m_d\cdot d_{12}\cdot\dot{\alpha}\cdot\dot{\gamma} = 0 \end{aligned} \tag{2.5}$$

$$\ddot{v}\cdot m_d + 2\cdot m_d\cdot\dot{\gamma}\cdot\dot{u} + v\cdot\left(-\dot{\gamma}^2 m_d - \dot{\alpha}^2 m_d + k_{11} + \frac{F_{ax}}{a}\right) + u\cdot\left(\dot{\alpha}\cdot\dot{\beta}\cdot m_d\right) - \varphi_1\cdot k_{14} + \\ + m_d\cdot d_{12}\cdot\dot{\beta}\cdot\dot{\gamma} = 0 \tag{2.6}$$

$$\ddot{\varphi}_1\cdot I_d + \dot{\varphi}_2.\left(I_p\Omega + I_p\dot{\gamma} - 2I_d\dot{\gamma}\right) + \\ + \varphi_1\cdot\left(I_p\dot{\gamma}\cdot\Omega + k_{44} + I_p\dot{\gamma}^2 - I_d\dot{\gamma}^2 - I_p\dot{\beta}^2 + I_d\dot{\beta}^2 + \frac{F_{ax}\cdot a}{5{,}844}\right) + \\ + \varphi_2\cdot\left(I_p\dot{\alpha}\dot{\beta} - I_d\dot{\alpha}\dot{\beta}\right) - k_{14}\cdot v + I_p\cdot\dot{\beta}\left(\Omega + \dot{\gamma}\right) = 0 \tag{2.7}$$

$$\ddot{\varphi}_2\cdot I_d + \dot{\varphi}_1\cdot\left(-I_p\Omega - I_p\dot{\varphi}_3 - I_p\dot{\gamma} + 2I_d\dot{\gamma}\right) + \\ + \varphi_2\left(I_p\dot{\gamma}\cdot\Omega + k_{44} + I_p\dot{\gamma}^2 - I_d\dot{\gamma}^2 - I_p\dot{\alpha}^2 + I_d\dot{\alpha}^2 + \frac{F_{ax}\cdot a}{5{,}844}\right) + \\ + \varphi_1\left(I_p\dot{\alpha}\dot{\beta} - I_d\dot{\alpha}\dot{\beta}\right) + k_{14}u - I_p\dot{\alpha}\cdot\left(\Omega + \dot{\gamma}\right) = 0 \tag{2.8}$$

The matrix format for the equations (2.5), (2.6), (2.7) și (2.8) becomes

$$[M]\{\ddot{q}\} + \left(\Omega\cdot[G] + \dot{\gamma}\cdot[C_d]\right)\{\dot{q}\} + \left([K] + \dot{\alpha}^2[K_{d1}] + \dot{\beta}^2[K_{d2}] + \dot{\gamma}^2[K_{d3}] + \right. \\ \left. + \dot{\alpha}\dot{\beta}[K_{d4}] + \dot{\gamma}\cdot\Omega[K_{d5}] + F_{ax}\cdot[K_{ax}]\right)\{q\} - \{F\} = 0. \tag{2.9}$$

Using the notations

$$[C_{Tot}] = \Omega\cdot[G] + \dot{\gamma}\cdot[C_d], \tag{2.10}$$

$$[K_{Tot}] = [K] + \dot{\alpha}^2[K_{d1}] + \dot{\beta}^2[K_{d2}] + \dot{\gamma}^2[K_{d3}] + \dot{\alpha}\dot{\beta}[K_{d4}] + \dot{\gamma}\cdot\Omega[K_{d5}] + F_{ax}\cdot[K_{ax}]. \tag{2.11}$$

The motion equation can be written in a simplified format

$$[M]\{\ddot{q}\} + [C_{Tot}]\{\dot{q}\} + [K_{Tot}]\{q\} - \{F\} = \{0\}. \tag{2.12}$$

$$\text{Where } \{q\} = \{u, v, \varphi_1, \varphi_2\}^T. \tag{2.13}$$

To solve the above equation of motion, it is first observed that the term $\{F\}$ is constant and therefore the result will be composed of a constant solution to which is added the solution of the homogeneous system of equations. From the point of view of determining the dynamic characteristics such as the natural vibrational frequencies in the linear domain, it is sufficient to solve the system of homogeneous equations. It should be noted that the equilibrium position around which the dynamic evolution takes place is determined by solving in this case the static equation

$$[K_{Tot}]\{q\} = \{F\}. \tag{2.14}$$

The homogenous equation is solved using the following notations

$$\{X\} = \begin{Bmatrix} \dot{q} \\ q \end{Bmatrix}, \tag{2.15}$$

$$[A] = \begin{bmatrix} [M] & 0 \\ 0 & [I] \end{bmatrix}, \tag{2.16}$$

$$[B] = \begin{bmatrix} [C_T] & [K_T] \\ [-I] & 0 \end{bmatrix}, \tag{2.17}$$

and searching for a solution in the form

$$\{X\} = \{Y\} \cdot e^{\lambda \cdot t}, \ \{\dot{X}\} = \lambda \cdot \{Y\} \cdot e^{\lambda \cdot t} \ . \tag{2.18}$$

Therefore the homogenous part of the equation (2.12) becomes

$$[A]\{\dot{X}\} + [B]\{X\} = \{0\}. \tag{2.19}$$

Replacing (2.18) in (2.19), then multiplying by $-[A]^{-1}$ results

$$-\lambda \cdot \{Y\} \cdot e^{\lambda \cdot t} - [A]^{-1}[B]\{Y\} \cdot e^{\lambda \cdot t} = \{0\}. \tag{2.20}$$

After simplifying for the term $e^{\lambda \cdot t}$ the classical eigenvalue problem is obtained

$$-[A]^{-1}[B]\{Y\} = \lambda \cdot \{Y\}, \tag{2.21}$$

whose solution consists of pairs of complex numbers λ and pairs of column arrays of complex numbers $\{Y\}$. Each pair consists of a complex number (set of numbers) and its conjugate. To find the solution to the initial problem (2.12) retain the lower half $\{y\}$ of the eigenvectors represented by the column matrices $\{Y\}$ so that

$$\{q\}(t) = \{y\} \cdot e^{\lambda t} + \{y\}^* \cdot e^{\lambda^* t}. \tag{2.22}$$

The imaginary part of the eigenvalues λ represents the eigenvalues of vibration of the rotor and the column matrices $\{y\}$ represent the forms of vibration of the rotor.

2.2 THE INFLUENCE OF THE AXIAL FORCE TO THE ROTOR MOTION IN A NON-INERTIAL REFERENCE FRAME. THE ANALYTICAL FORMULATION.

An indirect source of stiffness change for beams can generally be the tensile or compressive force acting along the beam and which, like a violin string which by its tensile force varies its own vibrational frequency, can lead to substantial change in natural vibration frequencies.

Thus, the differential stiffness matrix is obtained, which expresses the contribution of the axial force to the displacement of the center of mass of the disc.

$$\left[K_{ax}\right] = F_{ax} \cdot \begin{bmatrix} \frac{1}{a} & 0 & 0 & 0 \\ 0 & \frac{1}{a} & 0 & 0 \\ 0 & 0 & \frac{a}{5.844} & 0 \\ 0 & 0 & 0 & \frac{a}{5.844} \end{bmatrix}. \tag{2.23}$$

2.3 THE INFLUENCE OF THE SHAFT TORQUE TO THE ROTOR MOTION IN A NON-INERTIAL REFERENCE FRAME. THE ANALYTICAL FORMULATION.

For slender shafts or when a very precise calculation is desired, it is important to consider the torque transmitted by the rotor and more precisely by the rotor shaft. The torque is a vector that maintains its coaxial direction with the axis of the bearings along the shaft. Consequently, when the shaft suffers bending deformations, the torque vector is decomposed into two components, one tangential to the rotor shaft and one perpendicular to the shaft. The perpendicular component of the torque acts in the direction of amplifying the shaft deformation thus apparently reducing the rigidity of the shaft. Basically, in the presence of a high torsional load, the shaft seems to soften, a phenomenon that can evolve, in the case of slender shafts, to torsional buckling and destruction of the shaft.

Regarding vibrations, because always the torque has the effect of amplifying the displacement in the lateral direction on which it exerts its influence will generate in the equation of motion a stiffness matrix with minus sign, which will reduce the rigidity of the shaft.

$$\left[K_{tor}\right]=-M_{tor}\cdot\begin{bmatrix}0 & \frac{a+2b}{3a^2b} & 0 & 0\\ \frac{a+2b}{3a^2b} & 0 & 0 & 0\\ 0 & 0 & 0 & 1\\ 0 & 0 & 1 & 0\end{bmatrix}. \tag{2.24}$$

2.4 THE INFLUENCE OF THE IMBALANCE TO THE ROTOR MOTION IN A NON-INERTIAL REFERENCE FRAME. THE ANALYTICAL FORMULATION.

To determine the force generated by the rotor imbalance in the non-inertial reference system, the kinetic energy of the imbalance will be determined. The notation $m_e\cdot e$ is used for the rotor imbalance. The imbalance does not possess potential energy and therefore the Lagrange equations are been formulated only with the help of kinetic energy. (2.1) (2.4). Finally,one can write the force given by the imbalance in the rotor

$$-\left\{F_{dez}\right\}=m_e e\cdot\begin{Bmatrix}\dot{\alpha}\dot{\beta}\sin\left(\Omega t\right)-\left[\left(\dot{\gamma}+\Omega\right)^2+\dot{\beta}^2\right]\cos\left(\Omega t\right)\\ \dot{\alpha}\dot{\beta}\cos\left(\Omega t\right)-\left[\left(\dot{\gamma}+\Omega\right)^2+\dot{\alpha}^2\right]\sin\left(\Omega t\right)\\ 0\end{Bmatrix}. \tag{2.25}$$

With this it is possible to calculate the frequency response of the rotor on the operating range in the non-inertial reference system. This cause of vibration will be discussed in detail in Chapter Five, for numerical applications.

Another important feature in the calculation of lateral displacements of the rotors is the deviation from the perpendicularity of the rotor discs in relation to the axis of the bearings. The study of the inclined disc placement in the rotor will not be treated in this thesis but is a topic that will be developed in a future paper.

CHAPTER 3

ROTORS CLASSIFICATION REGARDING THE SHAFT ELASTICITY RELATED TO THE BEARINGS

Generally, when the greatest deformations during operation occur in the rotor shaft, the rotor is called a "flexible rotor". In contrast to the case of the flexible rotor is the case where major deformations in the operation of the rotary machine occur at the level of the bearings, in which case the rotor is called "rigid rotor". For the purpose of analyzing and designing rotor assemblies, the critical speed diagram that can be expressed in terms of bearing stiffness or shaft slenderness is very useful. Both parameters have a direct impact on critical speeds.

To formulate the equation of motion it is observed from figure 1.1 that any force or moment acting at the center of mass of the rotor, acts first on the shaft and then through the shaft acts on the bearings. So the system can be modeled as a series of elastic elements according to the following figure.

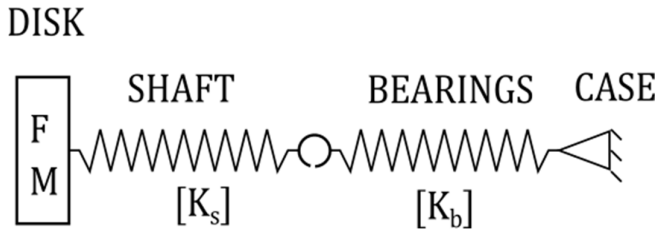

Figure 3.1. Schematic modeling of the rotor assembly regarding the stiffness matrices with highlighting the relationship between the stiffness matrices.

Thus, the equivalent elasticity can be expressed according to the spring series from which the stiffness matrix results $[K]$

$$[K]^{-1} = [K_s]^{-1} + [K_b]^{-1}, \quad \Rightarrow \quad [K] = \left([K_s]^{-1} + [K_b]^{-1}\right)^{-1}. \tag{3.1}$$

In the case of the "rigid rotor" the matrix $[K_s]$ has much larger terms than the matrix $[K_b]$ and in the equation (3.1) $[K_s]$ can be neglected without greatly affecting the final results in solving the equation of motion. In the other case when the rotor is called "flexible", the stiffness matrix of the bearings can be neglected.

The critical speed diagram is used to evaluate the characteristic of the flexible or rigid rotor in the preliminary design stage. It is constructed by varying the stiffness of the bearings (k_1,k_2) terms in $[K_b]$ or the slenderness of the shaft (L/d).[10, 11]

3.1 SIMPLIFIED FORMS OF THE TYPE RIGID SHAFT, RIGID BEARINGS. METHODS OF APPLICATION.

In practical approaches to industrial design problems, it is often indicated to simplify rotor modeling in order to eliminate the degrees of freedom corresponding to the deformation of the shaft or bearings. Based on the studies of Stroe I. and Crăița C. [10, 11], their method is brought to the fundamental level of the material point (eliminating the shape functions) and enriched with the author's contribution in simulating flexible rotors in addition to rigid ones. The theoretical reduction at the level of the material point opens the possibility of using the theory for any further development, especially in the field of the finite element which is based on the concept of "node" along with that of "element".

In the literature it is considered that a rotary machine shaft is flexible if it stores more than 70% of the potential vibration energy of the rotary machine and it is considered that the shaft is rigid if the percentage potential energy in the shaft is less than 30% of the total energy at vibration. [12] If we have the potential energy in the shaft between 30% and 70% of the total vibration energy then the shaft is considered as an "intermediate shaft". Depending on the application, each type can be desirable or avoided. Contrary to intuition, a robust rotary machine will not automatically have rigid bearings. In general, the flexibility given to the bearings leads to an increased reliability for the rotary machine. [13].

Considering the elasticity of the series of the two subassemblies, the shaft subassembly and the bearing subassembly according to the figure above, the stiffness matrix of the entire rotor assembly is obtained.

$$\left[K_{sb}\right]^{-1}=\left[K_s\right]^{-1}+\left[K_b\right]^{-1},\quad\Rightarrow\quad\left[K_{sb}\right]=\left(\left[K_s\right]^{-1}+\left[K_b\right]^{-1}\right)^{-1}. \tag{3.2}$$

This reasoning can be encoded as a Boolean vector

$$RF=\left[b_1\ b_2\right] \tag{3.3}$$

in which the variables b_1 and b_2 and can take the values 1 or 0 and with their help we can rewrite the equation (3.2) so that we have

$$\begin{aligned}&\left[K_{sb}\right]=\left(b_1\cdot\left[K_s\right]^{-1}+b_2\cdot\left[K_b\right]^{-1}\right)^{-1}.\\&RF=\left[1,0\right]\ \Rightarrow\ \text{flexible rotor,}\\&RF=\left[0,1\right]\ \Rightarrow\ \text{rigid rotor,}\\&RF=\left[1,1\right]\ \Rightarrow\ \text{intermediary rotor.}\end{aligned} \tag{3.4}$$

To assess potential energy the following relations are used

$$V_s=1/2\cdot\left\{F\right\}^T\left[K_s\right]^{-1}\left\{F\right\},\ \ V_b=1/2\cdot\left\{F\right\}^T\left[K_b\right]^{-1}\left\{F\right\} \tag{3.5}$$

$$V_s\%=\frac{V_s}{V_s+V_b}\cdot100,\qquad V_b\%=\frac{V_b}{V_s+V_b}\cdot100. \tag{3.6}$$

It is observed from (3.4) that if we have a rigid or flexible rotor then the equivalent stiffness matrix will be the stiffness matrix of the bearings respectively of the shaft. Finally the equation of motion in non-inertial reference system (2.9) can be rewritten considering (3.4)

$$\begin{aligned}\left[M\right]\left\{\ddot{q}\right\}+\left(\Omega\cdot\left[G\right]+\dot{\gamma}\cdot\left[C_d\right]\right)\left\{\dot{q}\right\}+\left(\left[K_{sb}\right]+\dot{\alpha}^2\left[K_{d1}\right]+\dot{\beta}^2\left[K_{d2}\right]+\dot{\gamma}^2\left[K_{d3}\right]+\right.\\\left.+\dot{\alpha}\dot{\beta}\left[K_{d4}\right]+\dot{\gamma}\cdot\Omega\left[K_{d5}\right]+F_{ax}\cdot\left[K_{ax}\right]\right)\left\{q\right\}-\left\{F\right\}=0.\end{aligned} \tag{3.7}$$

3.2 THE SIMULATION OF THE ROTORS WITH A NONLINEAR ELASTIC CHARACTERISTIC.

At present, the usual calculation algorithms regarding the natural frequencies of rotary machines are calculation algorithms in the linear field. Thus, in order to simulate the operation of the rotor, the linearization of the differential equations is done.

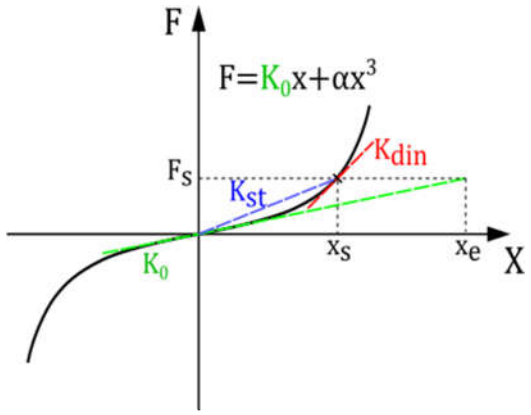

Figure 3.2. Elastic characteristic of a nonlinear bearing modeled as a third degree polinomial.

Due to the difficulty in obtaining results using nonlinear algorithms, the use of linear computational algorithms is always preferred as much as possible.

From a practical point of view, one of the simplest representations of a nonlinear characteristic is a third degree polynomial according to figure 3.2. Following figure 3.2 it is observed that the slope of the tangent for x = 0 represents the rigidity usually used, in the hypothesis of small displacements, in the linear calculation both static and dynamic. If the bearing is loaded with a relatively high static force Fs then the stiffness of the bearing can no longer be approximated by the tangent at x = 0 with the slope K_0 but a correction factor is used $\alpha \cdot x^2$ which adds up to K_0, depending on the displacement performed.

$$\begin{aligned} K_{st} &= K_0 + \alpha \cdot x^2, \\ F_s &= K_{st} \cdot x_s = \left(K_0 + \alpha \cdot x_s^{\,2}\right) \cdot x_s = K_0 x_s + \alpha \cdot x_s^{\,3} \end{aligned} \tag{3.8}$$

When analyzing the entire rotor and using the matrix notation

$$[K_{st}] = [K_0] + [K_G], \tag{3.9}$$

where the matrix $[K_G]$ is a correction matrix of the linear formulation and is called the geometric stiffness matrix.

$$K_{din} = \left(\frac{dF}{dx}\right)_{x=x_s} = \left(\frac{d}{dx}\left(K_0 x + \alpha \cdot x^3\right)\right)_{x=x_s} = K_0 + 3\alpha \cdot x_s^{\,2}. \tag{3.10}$$

From the above equation (3.10) it is obvious that the correction factor $3\alpha \cdot x_s^2$ must also be added to K0 which is usually used for linear calculation. When the calculation on the whole rotor assembly with all bearings is considered, the matrix form is used:

$$[K_{din}] = [K_0] + [K_D], \tag{3.11}$$

where the matrix $[K_D]$ is the differential stiffness matrix used for the linear dynamic calculation corresponding to the displacement xs and it encompasses all the correction factors corresponding to all nonlinear bearings.

Figure 3.3 below shows schematically the calculation steps involved in the presence of non-linear bearing.

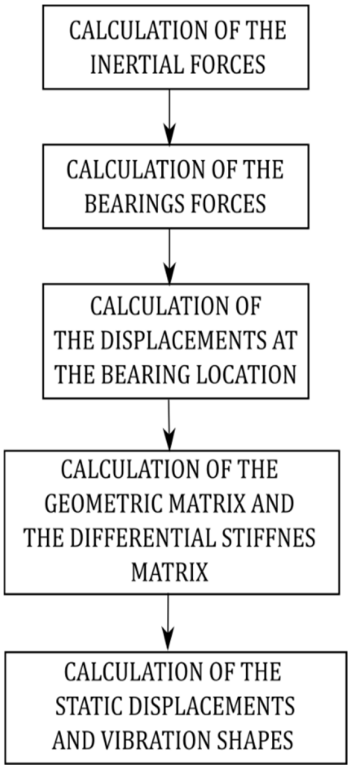

Figure 3.3. Calculation procedure for the case of a rotor with preload.

Full resolution in the case of rotors with nonlinear elastic characteristic can be done using iterative numerical methods over time such as Wilson-theta modified for nonlinear elastic characteristics. For this purpose, the author created a nonlinear solver that is used in the simulations that are shown below. The basic idea of iterative methods in general is to approximate the differential equation by Taylor series. Starting from this basic idea and adding other numerical techniques, the solvers based on the Runge-Kutta or Wilson-theta method are obtained.

3.2.1 Vibration without preload

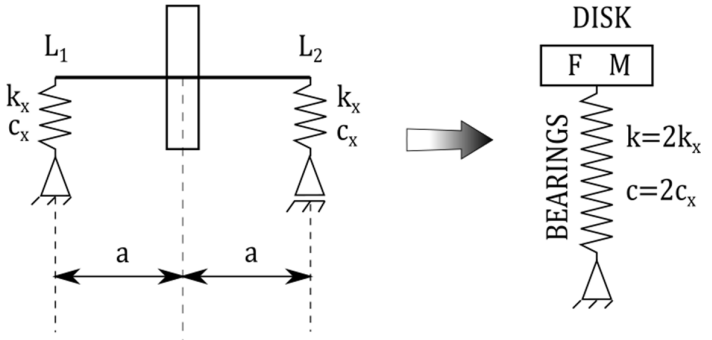

Figure 3.4. The reduction of the rigid shaft rotor type to an equivalent spring with mass.

In the case without preload there are no constant forces such as its own weight acting on the rotor. It is considered that the only force acting is one with sinusoidal characteristic such as centrifugal force due to rotor imbalance. Next, a preload is added. For the preload a lateral acceleration of 9.8 m/s^2 was choose to demonstrate the wider application beyond the non-inertial and regarding all the inertial cases considering the gravity.

Practical application.

Consider the same rotor in Figure 1.1, a=b, $|O_1O_2|=d_{12}=0$. Operating speed is between 0 and 3000 rpm. Consider the rigid shaft with negligible mass in relation to the disc. The mass of the disc is m = 259.16 Kg. Consider the bearing stiffness K = 1E7 [N / m], cubic stiffness α = 6E14, damping C = 25 [N / m], rotor imbalance me = 5.1e-4 [Kg.m] and lateral static force Fst = $m_d \cdot 9.8$ [N]. (applied in the case with preload)

It is desired to calculate the frequency response, in the inertial reference system for comparison and in the non-inertial system with preload.

Thus, in the present case when the characteristics of the bearings are homogeneous it is sufficient to solve the equation in the Ox direction.

The equation of motion for the inertial case is

$$m \cdot \ddot{x} + c \cdot \dot{x} + k \cdot x + \alpha \cdot x^3 = me \cdot \omega^2 \cdot \cos(\omega \cdot t) \tag{3.12}$$

In the following, several values of the imbalance were considered in ascending order in order to highlight the evolution of the resonance domains of the rotor. It was found that, unlike the linear case, the range in which the vibration with high amplitudes takes place is much larger in direct relation to the magnitude of the sinusoidal force (centrifugal force given by the rotor imbalance). In addition to this phenomenon, there is also the phenomenon of higher harmonics by which a harmonic force with a certain oscillation frequency produces the resonance of the rotor not only at that frequency but also at its multiples. For example, when the rotor is excited with a force varying by 44 Hz, the rotor will vibrate with a frequency of 88 Hz, although the amplitude corresponding to the vibration at 88 Hz is much smaller than that corresponding to the frequency of 44 Hz.

Table 3.1. Maximum vibration amplitudes for increasing and decreasing rotational speed.

No.case	Val. imbal. [Kg·m]	Max freq. ascend. [Hz]	Max freq. descend [Hz]	Max amplit. ascend [mm]	Max amplit. descend [mm]
1	1.0E-5	47	44	4.8E-5	1.1E-5
2	1.4E-5	52	44	9.1E-5	1.9E-5
3	1.6E-5	54	44	0.1	1.4E-5
4	1.8E-5	59	44	0.13	1.9E-5
5	2.0E-4	62	44	0.15	2.4E-5
6	2.2E-4	69	44	0.18	1.6E-5
7	2.4E-4	76	44	0.21	1.6E-5
8	2.6E-4	87	44	0.26	2.6E-5
9	2.8E-4	nominal	nominal	0.42	0.42

The table above summarizes the results described in the following figures. For case 1 (the associated figure below) the existence of a resonance range between the frequencies of 44 and 50 Hz is highlighted. The maximum vibration amplitude is 4.8E-5 m.

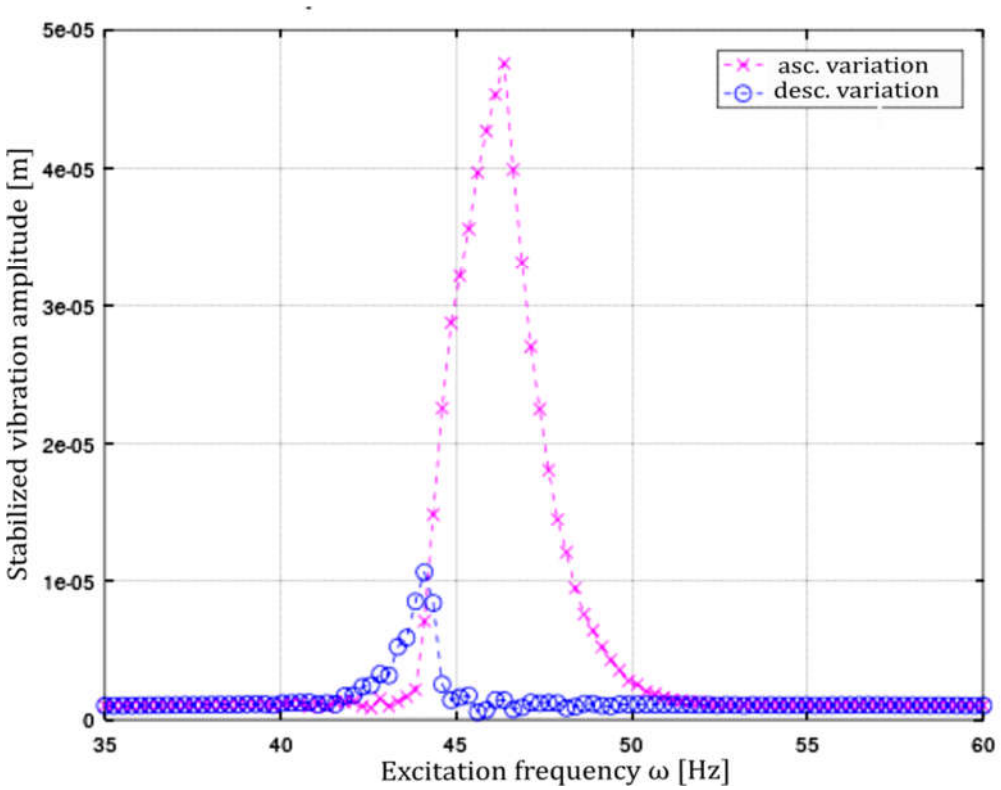

Figure 3.5. Case 1. The stabilized vibration amplitude in the presence of an imbalance of 1.0e-5 [Kg·m].

The different behavior of the rotor is observed when there is an increasing variation of the excitation force frequency compared to when there is a decreasing variation of the excitation force frequency. In the cases treated here being involved the rotor imbalance, the increase of the excitation force frequency takes place by simply increasing the rotational speed, respectively the decrease of the excitation frequency being achieved by decreasing the speed. For the case without preload nonlinear bearings with cubic polynomial characteristic,

the frequency response is manifested in the form of a lobe that increases to the right as the sinusoidal excitation force increases. In the case of rotors this force occurs due to the imbalance. In conclusion, for the rotors loaded with the unbalance force, in the case of non-linear bearings, the vibrations will manifest not at a certain frequency but in a frequency band that starts at the same value like in linear case and ends at a value that increases in proportion to the value of the load. The variation of the rotor disk response is done continuously on the left side of this frequency band and by a sudden jump on the right side. The sudden way this jump is made on the right side is attenuated in proportion to the existing damping in the bearings.

3.2.2 Vibration with preload

The case in the non-inertial reference system in which we have an acceleration on the Ox lateral direction of 9.8 m/s^2. The diagrams of speeds, critical frequencies in the two cases above will also be built.

The equation of motion for the non-inertial case with lateral acceleration a_L= 9,8 m/s^2 in the Ox direction is

$$m \cdot \ddot{x} + c \cdot \dot{x} + k \cdot x + \alpha \cdot x^3 = m \cdot a_L + me \cdot \omega^2 \cdot \cos(\omega \cdot t) \tag{3.13}$$

The inertial behavior deduced in point a) is maintained in the Oy direction because the acceleration acts only in the Ox direction and has no effect on the Oy direction.

Table 3.2. Maximum vibration amplitude for increasing and decreasing rotational speed.

No.case	Val. imbal. [Kg·m]	Max freq. ascend. [Hz]	Max freq. descend [Hz]	Max amplit. ascend [mm]	Max amplit. descend [mm]
1	1E-4	67	65	6.5E-5	0.13
2	2.6E-4	67	65	8.4E-5	0.14
3	5.1E-4	nominal	nominal	0.5	0.5

For the situation where there is a preload, the first major change occurs at the resonant frequency which undergoes a significant increase. From 44 Hz there is an increase to 65 Hz which is a percentage increase of 48%. Another surprising change is the change of the shape of the resonance domain characteristic from the "hardening" type to the "softening" type (characteristic for cases when alpha is negative in the equation (3.13)). Basically, there is an enlarged resonance range on the decreasing stage of the rotational speed and implicitly of the excitation frequency given by the centrifugal force of the imbalance. The associated figure below shows the widening to the left, in the range of lower frequencies, of the resonance range when there is an increase in the excitation force or the imbalance in the rotor. On the other hand, from the table above, it is observed that the maximum resonance frequency for the increasing speed variation is close to that for the decreasing speed variation with the increase of the imbalance. When they reach approximately the same value, there is an unlimited increase in the vibration amplitude with the speed. Practically the resonance range

extends to the entire rotational speed range larger than the speed corresponding to the frequency of 65 Hz.

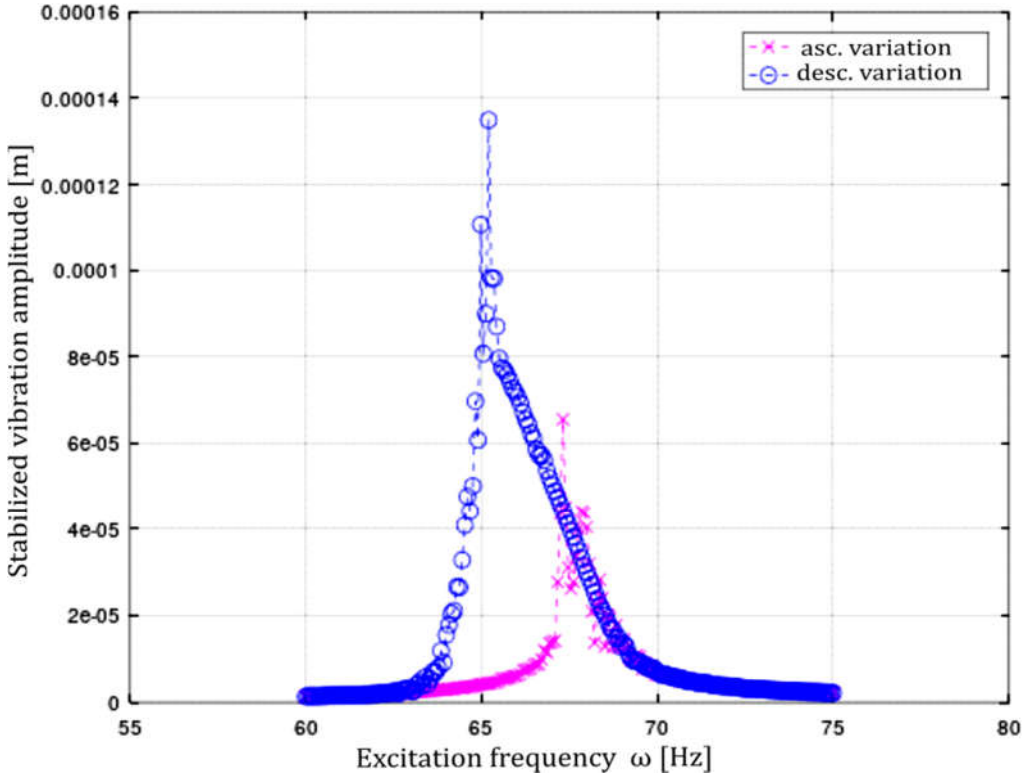

Figure 3.6. Case 1. The stabilized vibration amplitude in the presence of a constant lateral force of 2539.8 [N] and imbalance of 1.0e-4 [Kg·m].

CHAPTER 4

FINITE ELEMENT METHOD IN THE ANALYSIS OF THE ROTATING MACHINERY IN NON-INERTIAL SYSTEM

4.1 FORMULATION USING BEAM TYPE FINITE ELEMENT

In order to perform more detailed and accurate calculations in certain cases the matrices deduced in the previous chapter are developed for application in the field of finite elements. In general, the most used types of finite elements in the field of rotor dynamics are those of the Euler and Timoshenko type. Timoshenko-type elements can be considered as an improvement of the Euler-type ones with additional terms and coefficients for the simulation of shear strain phenomena along the rotor shaft fibers.

The basic idea in the finite element formulation is to start from a very thin section of shaft ds which is considered a very small disc at the coordinate s within one of the finite element that discretizes the rotor. For this very thin disc the characteristic sizes can be defined such as the mass of the disc m_s , the moment of geometric inertia I , the moment of mass inertia

on the diameter of the disc I_d and the moment of inertia along the axis of rotation of the disc I_p .

$$m_d = \rho \cdot \pi \cdot R^2 \cdot ds = \rho \cdot A \cdot ds. \tag{4.1}$$

$$I_d = \rho \cdot I \cdot ds, \tag{4.2}$$

$$I_p = 2 \cdot I_d. \tag{4.3}$$

For a small disk ds the kinetic energy is formulated identically according to the relations (2.2). In order to obtain the kinetic energy on the whole finite element, the integration is made in relation to the variable s along the entire length L_e of the finite element. Using the shape functions, the displacements at the coordinate s along the finite element are replaced by the displacements in the nodes at the ends of the finite element multiplied by the corresponding shape functions. Thus, in the end, the integration takes place on the functions of form. The Lagrange equation in matrix format has the form:

$$\frac{d}{dt}\left(\frac{\partial T}{\partial \{\dot{q}_e\}}\right) - \frac{\partial V}{\partial \{q_e\}} = \{0\}. \tag{4.4}$$

Integrating the energy for one finite element using the Lagrangean formulation is leading to terms of the type described below.(4.6)(4.7)

With regard to potential energy, a formulation valid for the Timoshenko type bar and implicitly for the Euler type bar is according to [12]

$$\begin{aligned} V &= \frac{1}{2}\{q_e\}^T \left(\left[K^e\right] + \left[K^e_{ax}\right]\right)\{q_e\} \\ \left[K^e\right] &= \left[K^e_b\right] + \left[K^e_\beta\right] \end{aligned} \tag{4.5}$$

On the other hand, the following terms take the form of kinetic energy, which take the form of additional stiffness matrices:

$$\left[K^e_{di}\right]\{q_e\} = \int_0^{L_e} \left(\left[\Psi(s)\right]^T \cdot \left[K_{dsi}\right] \cdot \left[\Psi(s)\right]\right)\{q_e\}, \; i = 1...5. \tag{4.6}$$

$$\begin{aligned} \left[K^e_{d1}\right] = -\rho A \int_0^{L_e} \left(\left[\Psi(s)\right]^T \cdot \begin{bmatrix} 0 & 0 & 0 & 0 \\ 0 & 1 & 0 & 0 \\ 0 & 0 & 0 & 0 \\ 0 & 0 & 0 & 0 \end{bmatrix} \cdot \left[\Psi(s)\right] \right) ds - \\ - \rho I \int_0^{L_e} \left(\left[\Psi(s)\right]^T \cdot \begin{bmatrix} 0 & 0 & 0 & 0 \\ 0 & 0 & 0 & 0 \\ 0 & 0 & 0 & 0 \\ 0 & 0 & 0 & 1 \end{bmatrix} \cdot \left[\Psi(s)\right] \right) ds. \end{aligned} \tag{4.7}$$

Similarly, using the same methodology, we obtain the expressions of the other non-inertial stiffness matrices associated with the finite element formulation, detailed in the thesis.

4.2 FORMULATION OF THE EQUATIONS WHICH GOVERNS THE INFLUENCE OF THE TORQUE OVER THE ROTOR SHAFT.

In the case of complex structures it is difficult to add the forces that are applied in the nodes of the finite elements in order to formulate the equation of motion. The principle of virtual displacements accompanied by the application of the D'Alembert principle contributes to the relatively easy obtaining of the equation of motion. Basically, the D'Alembert principle involves considering an inertial force that is in equilibrium with the other applied forces so that the sum of all the forces acting on the material point is zero. Next, the principle of virtual displacements is stated as follows: the mechanical work performed by a system of forces in equilibrium and which applies to a mechanical system (material point) is zero. Hamilton's principle is a solution for applying the principle of virtual travel. In its application, the cases of conservative forces differ from non-conservative ones. Conservative forces can be defined using a potential function which makes the mechanical work done by them to move the material point (node) independent of the trajectory followed between the initial and final position (which are considered fixed) and can be determined only by knowing potential function, initial and final position. Non-conservative forces are forces that transmit mechanical energy depending on the path on which the material point moves. This category can include dissipative forces such as friction and forces that bring energy from outside the mechanical system analyzed.

The Lagrange equation for one degree of freedom

$$\frac{d}{dt}\left(\frac{\partial T(\dot{u})}{\partial \dot{u}}\right)+\frac{\partial U}{\partial u}+c\dot{u}-f=0 \tag{4.8}$$

$$\boxed{\frac{d}{dt}\left(\frac{\partial T(\dot{u})}{\partial \dot{u}}\right)+\frac{\partial U}{\partial u}+\frac{\partial D}{\partial \dot{u}}-f=0} \tag{4.9}$$

Where with D is noted the dissipative function $D=\frac{1}{2}c\dot{u}^2$.

4.3 THE TIMOSHENKO BEAM THEORY

The energy using the strains column matrix is

$$U_e = \frac{1}{2}\begin{bmatrix} u_1 \\ v_1 \\ \theta_{x1} \\ \theta_{y1} \\ u_2 \\ v_2 \\ \theta_{x2} \\ \theta_{y2} \end{bmatrix}^T \begin{bmatrix} k_{11} & . & . & . & . & . & . & k_{18} \\ . & . & & & & & & . \\ . & & . & & & & & . \\ . & & & . & & & & . \\ . & & & & . & & & . \\ . & & & & & . & & . \\ . & & & & & & . & . \\ k_{81} & . & . & . & . & . & . & k_{88} \end{bmatrix} \begin{bmatrix} u_1 \\ v_1 \\ \theta_{x1} \\ \theta_{y1} \\ u_2 \\ v_2 \\ \theta_{x2} \\ \theta_{y2} \end{bmatrix} \qquad (4.10)$$

where the middle matrix represents the stiffness matrix K in Timoshenko formulation.

$$K_e = \frac{EI}{(1+\Phi)l^3}\begin{bmatrix} 12 & 0 & 0 & 6l & -12 & 0 & 0 & 6l \\ 0 & 12 & -6l & 0 & 0 & -12 & -6l & 0 \\ 0 & -6l & l^2(4+\Phi) & 0 & 0 & 6l & l^2(2-\Phi) & 0 \\ 6l & 0 & 0 & l^2(4+\Phi) & -6l & 0 & 0 & l^2(2-\Phi) \\ -12 & 0 & 0 & -6l & 12 & 0 & 0 & -6l \\ 0 & -12 & 6l & 0 & 0 & 12 & 6l & 0 \\ 0 & -6l & l^2(2-\Phi) & 0 & 0 & 6l & l^2(4+\Phi) & 0 \\ 6l & 0 & 0 & l^2(2-\Phi) & -6l & 0 & 0 & l^2(4+\Phi) \end{bmatrix} \qquad (4.11)$$

4.4 THE INFLUENCE OF THE TORQUE OVER THE LATERAL VIBRATION FREQUENCIES OF THE BEAM IN THE TIMOSHENKO FORMULATION

A requirement by practical applications is the ability to calculate the lateral vibration frequencies depending on the torque transmitted through the respective shaft. At the beginning of the development of the rotordynamics theory Greenhill, in 1883 [14] concludes that the torque does not influence the critical frequencies of the shafts. This simplifying hypothesis is not generally valid and later in 1921 Southwell and Gough [15] show that there are particular cases for which the torque leads to a decrease in critical vibration frequencies. In this regard, pioneering work was carried out especially by Golomb M. and Rosemberg R.M. [16] through the systematic activity in the experimental field and later by Eshleman and Eubanks through the theorizing efforts they carried out [17].

Thus Eshleman and Eubanks are the first to carry out a valid general systematic study to determine the areas of operation in which the effects of torque must be considered. Therefore, they developed and published the results of their study using dimensionless quantities related to the length and radius of the rotor shafts they studied using the so-called slenderness coefficient:

$$r = \frac{R}{2L} \tag{4.12}$$

As a working principle, Eshleman and Eubanks used the parallelogram rule to decompose the torque vector after the two directions of the finite element of the bar: the direction of the shear axis (which is perpendicular to the face of the finite element) and the direction corresponding to the face plane of the finite element.(see the figures below) Consider the torque T applied to the end of the finite element of length *l* and the direction of rotation in the direction of the Oz axis. The method published by author [18] is developed.

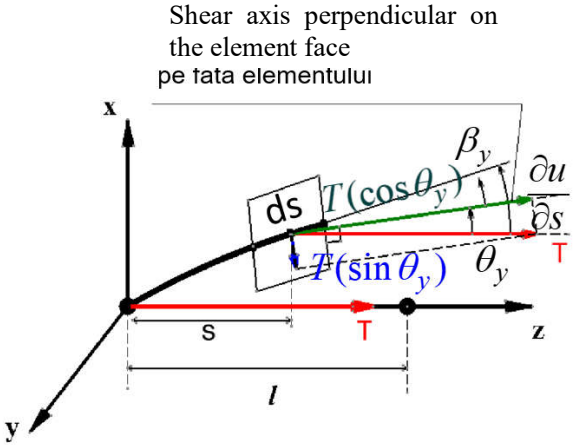

Figure 4.1. Moments and forces developed on the bar finite element

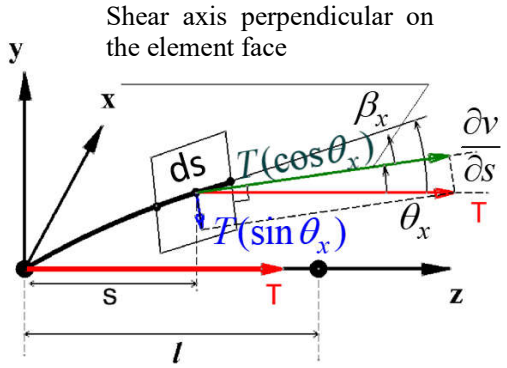

Figure 4.2. Moments and forces developed on the bar finite element

In order to define the equation of motion of the element, the generalized Hamiltonian principle is used in this case. As the torque is non-conservative, the Lagrange principle cannot be applied in this case. Thus we have:

$$\delta\int_{t1}^{t2}(K^e - P^e)dt + \int_{t1}^{t2}\delta W^e dt = 0 \tag{4.13}$$

The last term in the above equation is defined below using the notations:

$$T\theta_x = M_{tx} \tag{4.14}$$

$$T\theta_y = M_{ty} \tag{4.15}$$

$$\delta W^e = \int_0^l \left(-\delta\frac{\partial^2 v}{\partial s^2}M_{tx} + \delta\frac{\partial^2 u}{\partial s^2}M_{ty} \right) ds \tag{4.16}$$

Arranged in matrix form:

$$\delta W^e = \int_0^l \left(T\begin{bmatrix}\frac{\partial u}{\partial s}\\ \frac{\partial v}{\partial s}\end{bmatrix}^T \begin{bmatrix}0 & -1\\ 1 & 0\end{bmatrix}\begin{bmatrix}\delta\frac{\partial^2 u}{\partial s^2}\\ \delta\frac{\partial^2 v}{\partial s^2}\end{bmatrix}\right) ds + \int_0^l \left(T\frac{\Phi l^2}{12}\begin{bmatrix}\frac{\partial^3 u}{\partial s^3}\\ \frac{\partial^3 v}{\partial s^3}\end{bmatrix}^T \begin{bmatrix}0 & -1\\ 1 & 0\end{bmatrix}\begin{bmatrix}\delta\frac{\partial^2 u}{\partial s^2}\\ \delta\frac{\partial^2 v}{\partial s^2}\end{bmatrix}\right) ds \tag{4.17}$$

Considering the notation $\Psi(s) = \begin{bmatrix}\Psi_T(s)\\ \Psi_R(s)\end{bmatrix}$ with the part corresponding to the translational displacements $\Psi_T(s)$ and noting the vector of the displacements at the ends of the finite element with q^e, the equation (4.17) turns:

$$\begin{aligned}\delta W^e = \{\mathrm{q}^e\}^T \int_0^l \left(T[\Psi_T(s)']^T \begin{bmatrix}0 & -1\\ 1 & 0\end{bmatrix}[\Psi_T(s)'']\right) ds\cdot\delta\{\mathrm{q}^e\} + \\ + \{\mathrm{q}^e\}^T \int_0^l \left(T\frac{\Phi l^2}{12}[\Psi_T(s)''']^T \begin{bmatrix}0 & -1\\ 1 & 0\end{bmatrix}[\Psi_T(s)'']\right) ds\cdot\delta\{\mathrm{q}^e\}\end{aligned} \tag{4.18}$$

$$\delta W^e = \left[\int_0^l \left(T[\Psi_T(s)'']^T \begin{bmatrix} 0 & 1 \\ -1 & 0 \end{bmatrix} [\Psi_T(s)'] \right) ds \cdot \{q^e\} \right]^T \cdot \delta\{q^e\} + \\ + \left[\int_0^l \left(T\frac{\Phi l^2}{12}[\Psi_T(s)'']^T \begin{bmatrix} 0 & 1 \\ -1 & 0 \end{bmatrix} [\Psi_T(s)'''] \right) ds \cdot \{q^e\} \right]^T \cdot \delta\{q^e\} \tag{4.19}$$

Using the notation:

$$K_{T\alpha} = \int_0^l \left(T[\Psi_T(s)'']^T \begin{bmatrix} 0 & 1 \\ -1 & 0 \end{bmatrix} [\Psi_T(s)'] \right) ds \tag{4.20}$$

$$K_{T\beta} = \int_0^l \left(T\frac{\Phi l^2}{12}[\Psi_T(s)'']^T \begin{bmatrix} 0 & 1 \\ -1 & 0 \end{bmatrix} [\Psi_T(s)'''] \right) ds \tag{4.21}$$

The equation (4.19) becomes

$$\delta W^e = \left[K_{T\alpha} \cdot \{q^e\}\right]^T \cdot \delta\{q^e\} + \left[K_{T\beta} \cdot \{q^e\}\right]^T \cdot \delta\{q^e\} \tag{4.22}$$

$$\boxed{\delta W^e = \left[\left(K_{T\alpha} + K_{T\beta}\right) \cdot \{q^e\}\right]^T \cdot \delta\{q^e\}} \tag{4.23}$$

where $K_{T\alpha}$ and $K_{T\beta}$ are the stiffness matrices given by the torque transmitted through the shaft analyzed according to the theory of bending the bar in the form of Timoshenko.

4.5 CRITICAL TORQUE CALCULATION FOR THE TORSIONAL BUCKLING OF THE BEAMS USING TIMOSHENKO BEAM FORMULATION

Compression and torsional buckling of the rotor shaft can be discussed. The buckling limit at compression can also be determined using the stiffness matrix [19] published by Kosmatka $\left[K_A^e\right]$ in the formulation of the Timoshenko bar. Practically when the terms of the stiffness matrix Timoshenko $\left[K_B^e\right]$ are canceled by the terms of the stiffness matrix Kosmatka, the bending stiffness of the shaft becomes zero and its buckling takes place. On the other hand, from the point of view of torsional buckling, similarly when the terms of the stiffness matrix Timoshenko are canceled by the terms of the stiffness matrix

given by the torsional moment $\left[K_T^e\right]$ the torsional buckling takes place. Thus, in the formulation of the equation of motion we have for the formulation in inertial system and simple torsional load,

$$\left[K^e\right]=\left[K_B^e\right]-\left[K_T^e\right] \text{ , } \left[K_T^e\right]=\left[K_{T\alpha}^e\right]+\left[K_{T\beta}^e\right]. \tag{4.24}$$

The index e denotes the formulation at the finite element level. Considering the torque denoted by the T

$$T=k\frac{EI}{L} \tag{4.25}$$

where EI is the bending stiffness of the rotor and L is the distance between the bearings supporting the rotor, the following formulation can be made in static mode

$$\left[K\right]\{q\}=0 \tag{4.26}$$

$$\left(\left[K_B\right]-\left[K_T\right]\right)\{q\}=0 \tag{4.27}$$

The stiffness matrix given by the torque corresponding to the buckling limit is

$$\left[K_T^F\right]=\frac{1}{k}\left[K_T\right] \tag{4.28}$$

Thus the equation (4.27) becomes

$$\left(\left[K_B\right]-k\left[K_T^F\right]\right)\{q\}=0 \tag{4.29}$$

$$\left(\left[K_T^F\right]^{-1}\left[K_B\right]-k\left[I\right]\right)\{q\}=0 \tag{4.30}$$

Thus, the equation (4.30) corresponds to a problem with eigenvectors and eigenvalues where the values of k used in the equation (4.25) lead to finding the critical torques for the torsional buckling phenomenon. According to Ziegler [20] for rotors with simple shafts supported on short bearings $k_1=2\cdot\pi$ (it is mentioned that in Ziegler pag.126,127 is not included the number π in the coefficient k like in the work [20] $k=2$ which is later explicitly multiplied by π in order to obtain the formula (4.25)). This allows the calculation of the maximum value for the torque T from which the buckling phenomenon occurs.

If the rotor is in rotational motion, the stability at lateral displacements is also influenced by the gyroscopic forces. They can have a stabilizing influence on the tendency of lateral vibration if the precession takes place in the direction of rotation or destabilizing if the precession takes place in the opposite direction.

Thus for the general case, the equation of motion in the non-inertial reference system (2.9) becomes

$$[M]\{\ddot{q}\}+\left(\Omega\cdot[G]+\dot{\gamma}\cdot[C_d]\right)\{\dot{q}\}+\left([K]+\dot{\alpha}^2[K_{d1}]+\dot{\beta}^2[K_{d2}]+\dot{\gamma}^2[K_{d3}]+\right.$$
$$\left.+\dot{\alpha}\dot{\beta}[K_{d4}]+\dot{\gamma}\cdot\Omega[K_{d5}]+[K_A]-[K_T]\right)\{q\}-\{F\}=0. \tag{4.31}$$

similarly to the analytical formulation except that the meaning of the matrices is different, they are obtained by assembly techniques specific to the finite elements [12] of the matrices and vectors defined for each finite element and which are given in the relations, (4.7) -,(4.11),(4.24) deduced in previous chapters. Regarding the column matrix $\{F\}$ it should be mentioned that it can also include the influence of the imbalance deduced in (2.25) in addition to non-inertial forces.

One can observe that the term dependent on the torque $[K_T]$ negatively influences the bending stiffness of the rotor assembly. This influence becomes very important in the case of slender rotors and leads to a decrease to zero of the first critical lateral vibration frequency if the torque approaches the torsional buckling limit. The other vibration modes also record noticeable decreases in their own vibration frequencies.

4.6 CALCULATION IN THE LARGE DISPLACEMENTS CONTEXT

For the calculation of vibration forms and vibration frequencies in top areas such as aerospace, the simple vibration calculation using manufacturing geometry is not satisfactory. This is due to the fact that the parts that make up the turbomotors and in general the highly loaded components of the aerospace industry show a considerable change in geometry during operation [21] so that the forms of vibration undergo a substantial change. Also, the state of tension in the body of the parts as well as the acceleration fields to which they are subjected determine the considerable change of the vibration frequencies. [22, 23] A particular case is the combination of the above two effects, with an interactive change in the application of the loads depending on the deformation of the part. An eloquent example of this phenomenon is the change of the local direction of application of the centrifugal force depending to the strong deformation of the analyzed structure. The consequence of the variation of the rotor disk geometry as a function of speed is the variation of its mechanical characteristics such as moments of inertia $I_p(\Omega)$ and $I_d(\Omega)$. It follows that all matrices involving these terms will be speed dependent. Consequently the motion equation (4.31) becomes

$$\left[M(\Omega)\right]\{\ddot{q}\}+\left(\Omega\cdot\left[G(\Omega)\right]+\dot{\gamma}\cdot\left[C_d(\Omega)\right]\right)\{\dot{q}\}+$$
$$+\left([K]+\dot{\alpha}^2\left[K_{d1}(\Omega)\right]+\dot{\beta}^2\left[K_{d2}(\Omega)\right]+\dot{\gamma}^2\left[K_{d3}(\Omega)\right]+\right. \tag{4.32}$$
$$\left.+\dot{\alpha}\dot{\beta}\left[K_{d4}(\Omega)\right]+\dot{\gamma}\cdot\Omega\left[K_{d5}(\Omega)\right]+[K_A]-[K_T]\right)\{q\}-\{F(\Omega)\}=0.$$

Due to the speed dependence of the terms of the equation of motion, the critical speeds will be obtained iteratively. The value of the critical speed sought is estimated and then the matrices necessary for the calculation of the critical speed are obtained and the desired critical speed is calculated. The comparison of the estimated with the obtained value is done to verify the fit in the desired accuracy. If the required accuracy is not met, the calculation is resumed using the value calculated in the previous step as the estimated critical speed. The procedure is repeated until the desired calculation accuracy is reached.

CHAPTER 5

NUMERICAL APPLICATIONS

5.1 TWO REFERENCE CASES IN THE ROTORDYNAMICS LITERATURE

5.1.1 One disk rotor, analysis in an inertial reference system

The rotor shaft has a radius R = 0.01m and a length of 1.4m. The material from which the rotor is made is steel with density $\rho=7800Kg/m^3$ and modulus of elasticity $E=2\cdot10^{11}N/m^2$. The disc has a radius of 0.15 m and a thickness of 0.03 m.

For the disc imbalance are given the mass of the imbalance $m_e=10^{-4}kg$ and the distance d = 0.15 m resulting in $m_e\cdot d=1.5\cdot10^{-5}m\cdot Kg$.

At a distance of two thirds of the shaft length is located the bearing L_2 with elastic characteristics $k_{xx}=2\cdot10^5$ N/m, $k_{yy}=5\cdot10^5$ N/m and with damping $c_{xx}=40$ N/m, $c_{yy}=100$ N/m.

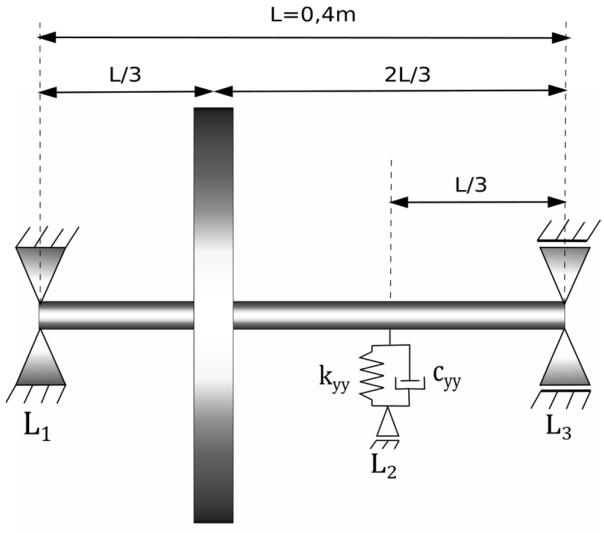

Figure 5.1. One disk and three bearings rotor.(Lalanne pag.191)

Six Timoshenko-type elements were used to discretize the rotor.

a) **Campbell diagram**

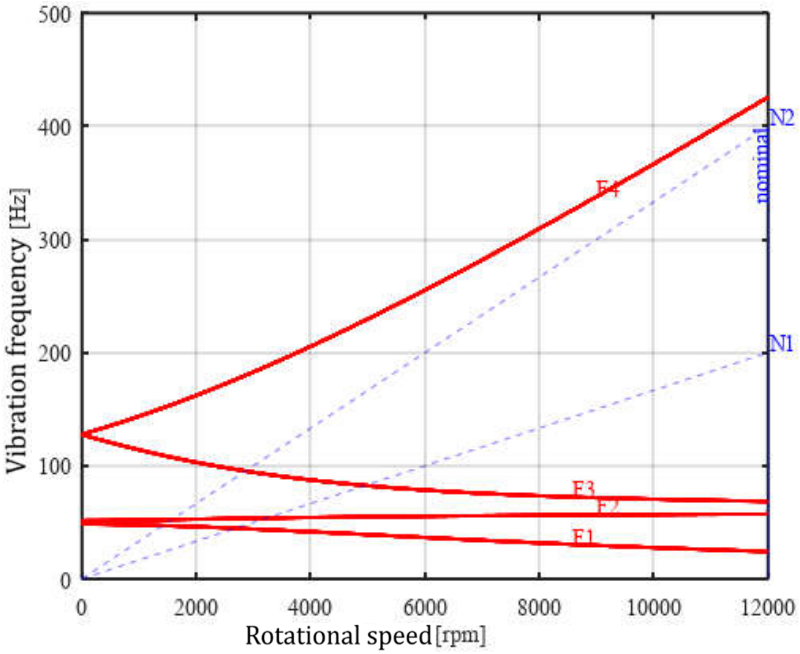

Figure 5.2. Campbell diagram in the inertial reference system (usual case).

b) Frequency response due to the imbalance load

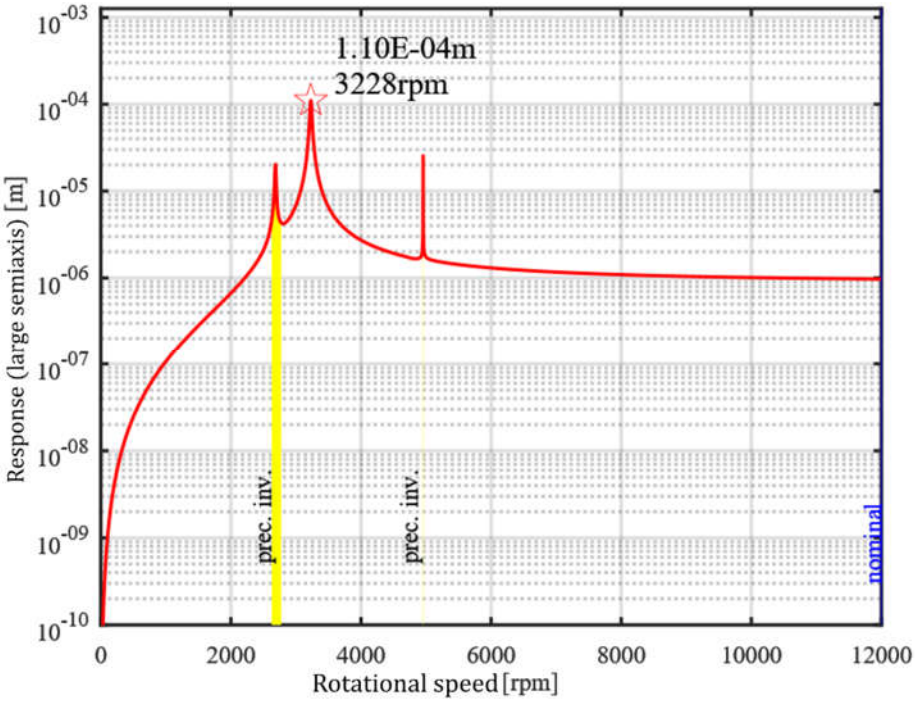

Figure 5.3. Maximum radial disk displacement due to the imbalance with the reverse precession zones marked with yellow (rev. prec. yellow band).

5.1.2 Three disks rotor, analysis in an inertial reference system

a) **Campbell diagram**

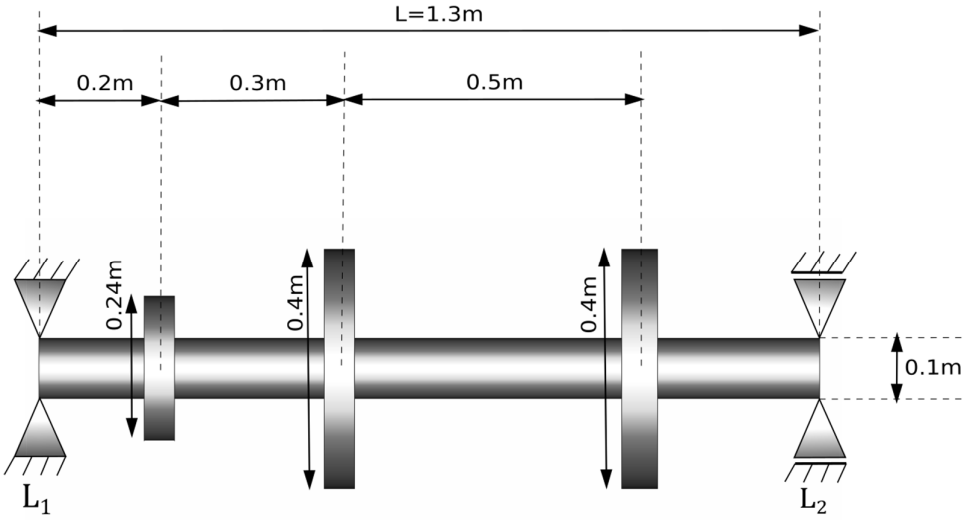

Figure 5.4. Three disks and two bearings rotor.(Lalanne pag.126)

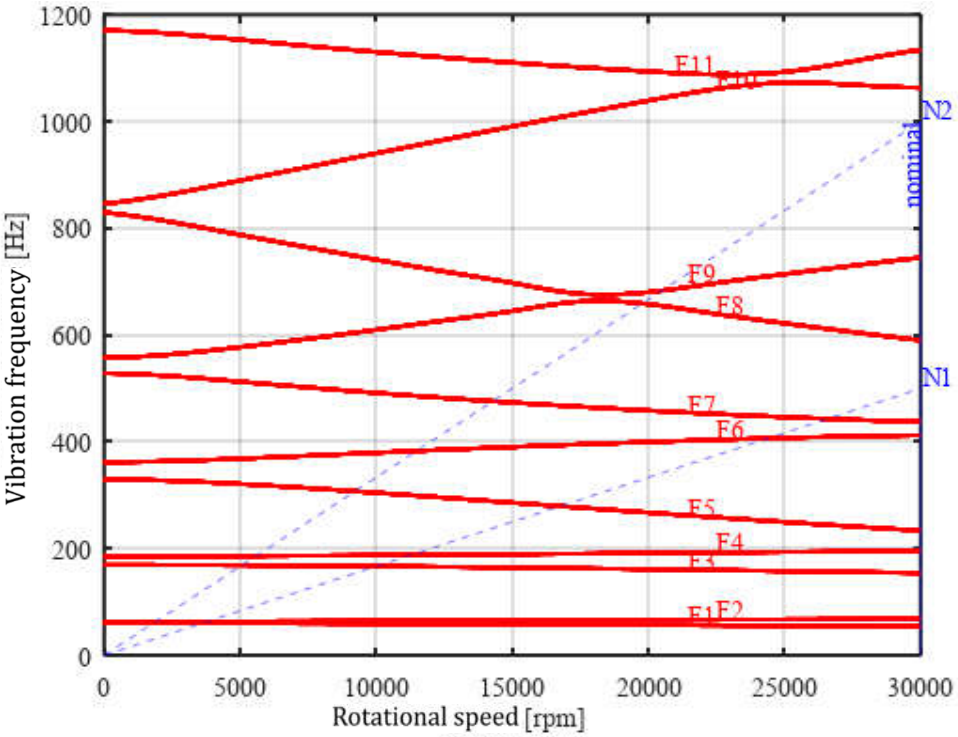

Figure 5.5. Campbell diagram in the inertial reference system (usual case).

The two bearings are anisotropic with the elastic characteristics $k_{xx}=5\cdot10^7$, $k_{yy}=7\cdot10^7$ and the damping $c_{xx}=5\cdot10^2$, $c_{yy}=7\cdot10^2$ different in the direction of the Ox axis from the Oy

axis. The material is steel with density ρ=7800Kg/m^3, modulus of elasticity E=2·10^{11} N/m and Poisson's ratio ν=0,3. Operating range is 0-30000rpm. The discretization with Timoshenko type bar finite elements is performed according to the one presented by Lalanne in [24] to allow the comparison of the results in the usual inertial frame of reference. The reason for choosing this calculation case is its wide use in the literature, which allows comparing the results obtained by the author with those already published and implicitly validating the starting model, and then assessing the author's original contributions to the current state of the art.

b) Frequency response due to the imbalance load

The calculation of the frequency response under the action of the synchronous force generated by the imbalance of the second rotor (denoted R2 in the previous figures) measured at the level of this rotor is shown in the figure below. The calculation of the radial maximum displacement highlights the existence of the seven local maxima corresponding to the seven critical velocities when the vibration lines intersect the excitation line N1. The values calculated for each critical speed and the associated vibration frequency are given in the first table below. For reference, the reference values provided by Lalanne for exactly the same rotor in the paper [24] are also reproduced. The relative error obtained in relation to the reference values is very small, being equal to or less than 0.2% except for the seventh critical speed at which the calculated maximum radial displacement has an error of 1.3% compared to the reference. The exact precession domains of the second disk R2 are highlighted exactly as well as the speeds at which there is no precession (the start and end speeds of the backward precession zones when the graph of the small half-axis, not showed here, tends to zero).

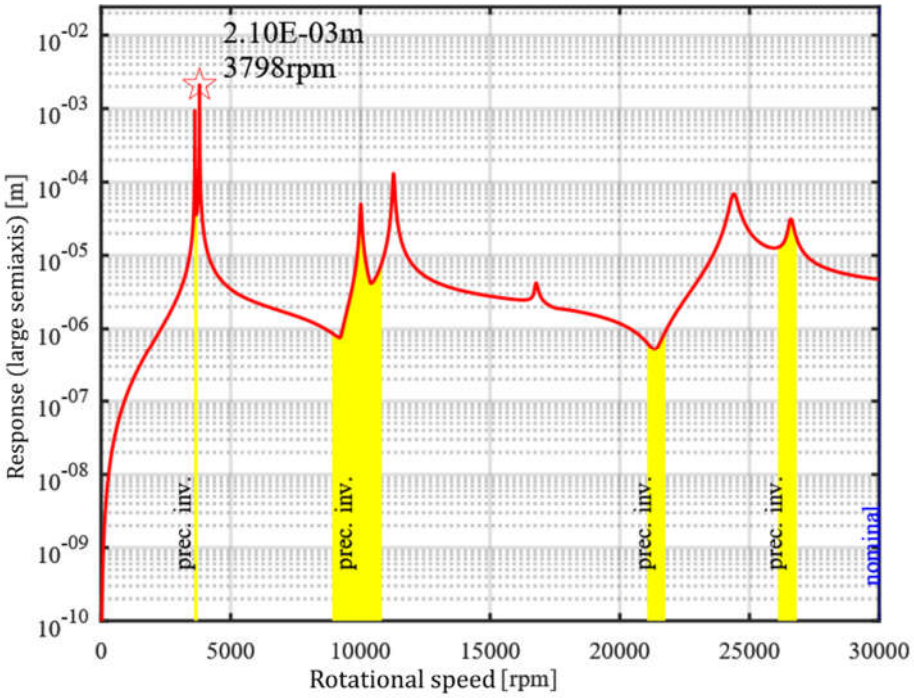

Figura 5.6. Maximum radial displacement of R2 disk due to the imbalance load with the marking of the backward precession domains (prec. inv. yellow band)

The preferential direction of vibration for each speed without precession is dictated by the inhomogeneous nature of the elasticity of the bearings in the Ox and Oy direction. Finally, the maximum radial displacement for the entire rotor of 2.2 mm (see the thesis) at node 8 at 3798rpm was calculated.

Table 5.1. Evaluation of calculation accuracy for critical frequencies and vibration amplitude

No. critical speed	Lalanne reference pag.131 table 6.3 [24]		Results obtained in the author implementation	
	Rotational speed [rpm]	Response [m]	Rotational speed [rpm] (error%)	Response [m] (error%)
1	3620.4	9.38E-04	3619.9 (0.0%)	9.38E-04 (0.0%)
2	3798.1	2.10E-03	3798 (0.0%)	2.10E-03 (0.0%)
3	10018	5.00E-05	10015 (0.0%)	5.00E-05 (0.0%)
4	11279	1.30E-04	11279 (0.0%)	1.30E-04 (0.0%)
5	16785	4.21E-06	16776 (0.1%)	4.20E-06 (0.2%)
6	24408	6.84E-05	24398 (0.0%)	6.85E-05 (0.1%)
7	26615	3.09E-05	26595 (0.1%)	3.13E-05 (1.3%)

5.2 ROTOR IN NON-INERTIAL REFERENCE SYSTEM SUBJECTED TO ACCELERATION IN THE BEARING'S AXIS DIRECTION

When an acceleration is applied in the axial direction, the Timoshenko formulation of the stiffness matrix is modified by adding an additional matrix called the differential stiffness matrix [24]. Thus, if a tension in the Timoshenko type bar elements occurs, there is an increase in the rigidity of the element, resulting in an increase in the fundamental vibrational frequency of the entire rotor assembly. When the acceleration is applied in the opposite direction to the previous case, there is a decrease in the stiffness of the bar element so that the fundamental vibration frequency decreases in proportion to the magnitude of the acceleration. In the case of rotors with slender shafts, this decrease can act until reaching the value of zero for the natural vibration frequency, which corresponds to the buckling of the rotor shaft. Another factor that influences the natural vibration frequency of the rotors is, as demonstrated in this thesis, the torque and thus the power conveyed by the rotary machine. *From this point of view, whenever the increase of the power transferred through the shaft of the rotary machine takes place, the fundamental frequency of vibration of the rotor decreases.*

5.2.1. One disk rotor

a) Case of compression stress: Acceleration in the direction of Oz = 30000 m/s².

The particularly high value of the acceleration was chosen to clearly show on the Campbell diagram the effect of the axial acceleration. For usual acceleration values it would be desirable to use slender rotor models such as the helicopter's anti-torque propeller shaft but these are not easy accessible in the literature published in the field of rotors.

In this case, the shaft is compressed. The fundamental vibration frequency is zero Hertz and that translates to buckling of the shaft.

b) Case of tensile stress: Acceleration in the direction of Oz Oz = -30000 m/s².

All its own frequencies undergo a noticeable increase due to the appearance of an inertial stretching force of the shaft.

5.2.2. Three disks rotor

a) Case of compression stress: Acceleration in the direction of Oz = 30000 m/s²

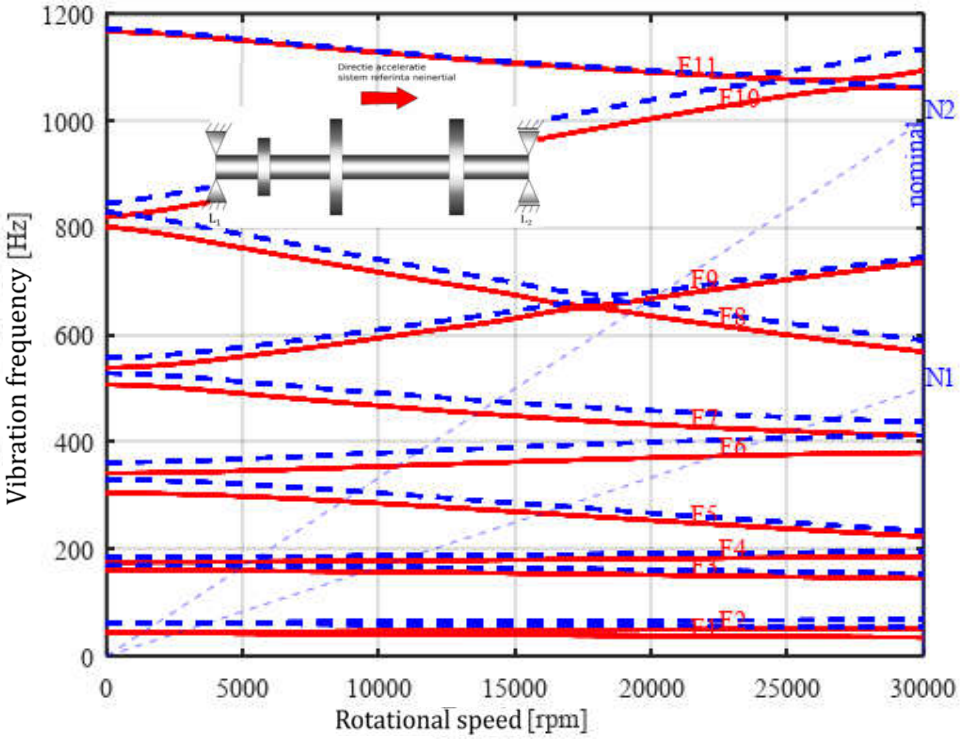

Figure 5.7. Campbell diagram in non-inertial reference system (a_z= 30000 m/s^2) With blue interrupted line is depicted the inertial case.

For the chosen three disk configuration, the shaft is very rigid and there is a moderate variation of the vibration lines due to the acceleration load applied along the axial direction. Thus maintaining the safety margin of 10%, the operating range in the vicinity of the nominal speed is 92 - 100%. This results in a 6% increase in this operating range compared to the inertial case.

b) Case of tensile stress: Acceleration in the direction of Oz = -30000 m/s².

In the case of the acceleration that determines the elongation of the shaft, there is an upward movement of the vibration lines in the Campbell diagram. This movement takes place in such a way that if the N1 / F7 intersection is checked, it is found that it no longer respects the required safety margin of 10%. It can thus be concluded that the operation of the rotary machine at nominal speed becomes dangerous and it is necessary to reduce the operating speed in the range of 64 - 78%. By tensioning, the rigidity of the shaft increases so that the bearings become more loaded to the vibrational movement than in the inertial case.

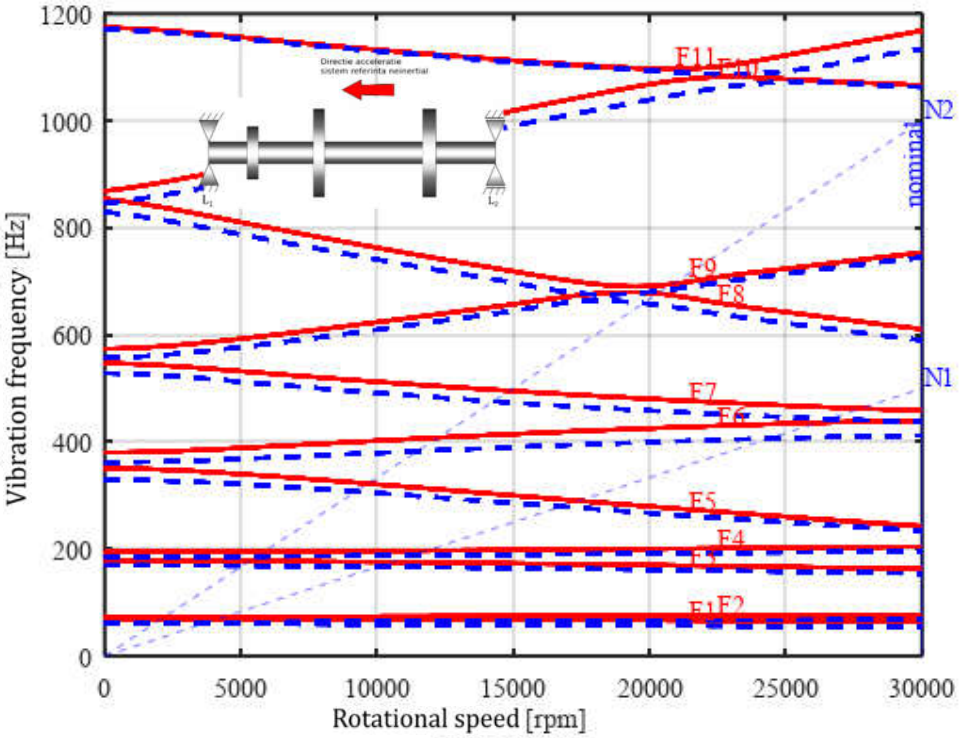

Figure 5.8. Campbell diagram in non-inertial reference system (a_z= -30000 m/s^2). With blue interrupted line is depicted the inertial case.

5.3 ROTOR IN NON-INERTIAL REFERENCE SYSTEM SUBJECTED TO ACCELERATIONS DUE TO A ROTATIONAL VECTOR PERPENDICULAR TO THE BEARING AXIS

5.3.1 One disk rotor, rotation around the axial bearing

$\left(\dot{\alpha} = 0rps, \dot{\beta} = 30rps, \dot{\gamma} = 0\right)$

a) Campbell diagram

In the case of the rotating machine in the reference system which rotates around the Oy axis passing through the radial axial bearing, from a quantitative point of view, the dominant effect is the shaft stretching which produces the increase of the frequencies of the vibration lines. From a qualitative point of view, the direct influence of the rotation of the non-inertial reference system is decisive, so that the vibration lines no longer start (at zero rotational speed) from two points corresponding to the two forms of vibration but start from four points. This division is due to the phenomenon called "spin softening" manifested for vibration in the plane perpendicular to the non-inertial system rotation vector.

b) Frequency response to imbalance load

The critical rotational speeds are shifting towards superior frequency values.

5.3.2 One disk rotor, rotation around the disk center of mass

$\left(\dot{\alpha} = 0rps, \dot{\beta} = 30rps, \dot{\gamma} = 0\right)$

If the non-inertial reference system originate in the center of mass of the disc, the stress in the shaft due to the inertial forces is minimal, practically negligible in this particular case. This makes it clear the effect of the rotation of the non-inertial system on the Campbell diagram. It is observed that the vibration lines corresponding to the same form of vibration no longer start from the same point at zero speed. This is due to the occurrence of the spin softening phenomenon in the plane perpendicular to the rotation vector of the non-inertial reference system Ox1y1z1.

a) Campbell diagram

The stress in the shaft is minimized. There is a slight decrease in the fundamental frequency.

b) Frequency response due to the imbalance load

The amplitude of the fundamental frequency vibration increases greatly.

5.3.3 One disk rotor, rotation around the opposite shaft end relating to the axial bearing $\left(\dot{\alpha}=0rps,\dot{\beta}=30rps,\dot{\gamma}=0\right)$

In this case the two phenomena contribution is to an apparent increase in the flexibility of the rotor shaft. In this configuration the axial force is negative, of compression, and therefore the contribution of the matrix $\left[K_A\right]$ is in the sense of decreasing the rigidity of the rotor.

a) Campbell diagram

An inertial compressive force occurs in the shaft. The fundamental frequency drops to zero Hertz thus signaling the buckling of the shaft.

b) Frequency response due to the imbalance load

Lateral movement of the rotor shaft at zero rotational speed is developing due to inertial forces and imbalance.

5.3.4 Three disks rotor, rotation around the axial bearing

$\left(\dot{\alpha}=0rps,\dot{\beta}=30rps,\dot{\gamma}=0\right)$

a) Campbell diagram

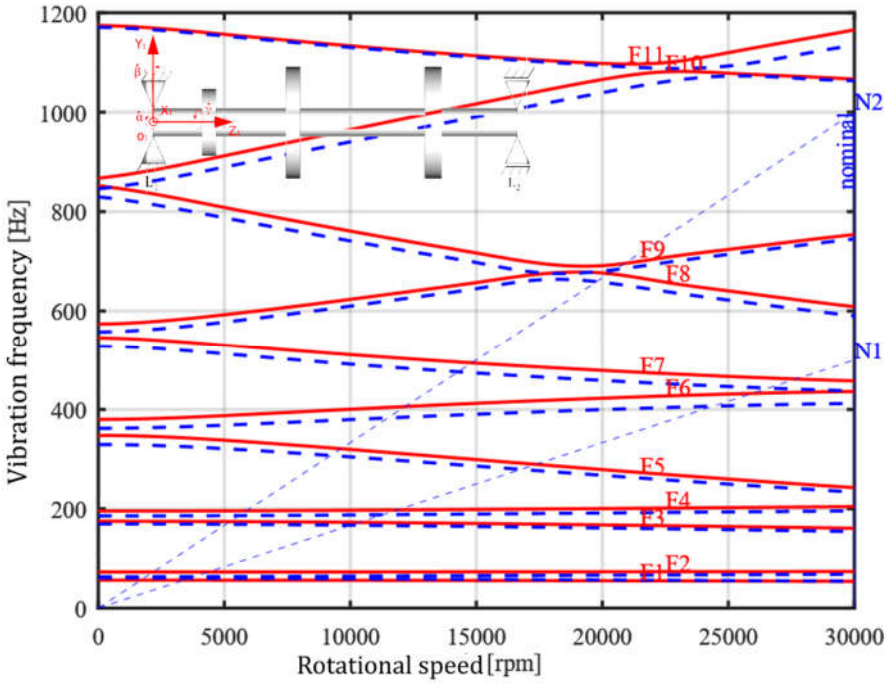

Figure 5.9. Campbell diagram in non-inertial reference system ($\dot{\beta}=30rps$). With blue interrupted line is depicted the inertial case.

For the case when the non-inertial reference system is located with the origin in the radial axial bearing the state of the axial tension is considerable. The Campbell diagram shows the slightly upward movement of the vibration lines except for the F1 line which is most sensitive to non-inertial system rotation according to an axis perpendicular to the bearing axis. It can be said that in the case of the F1 line the phenomenon of "spin softening" has a greater influence than the tension of the shaft.

b) Frequency response to the imbalance load

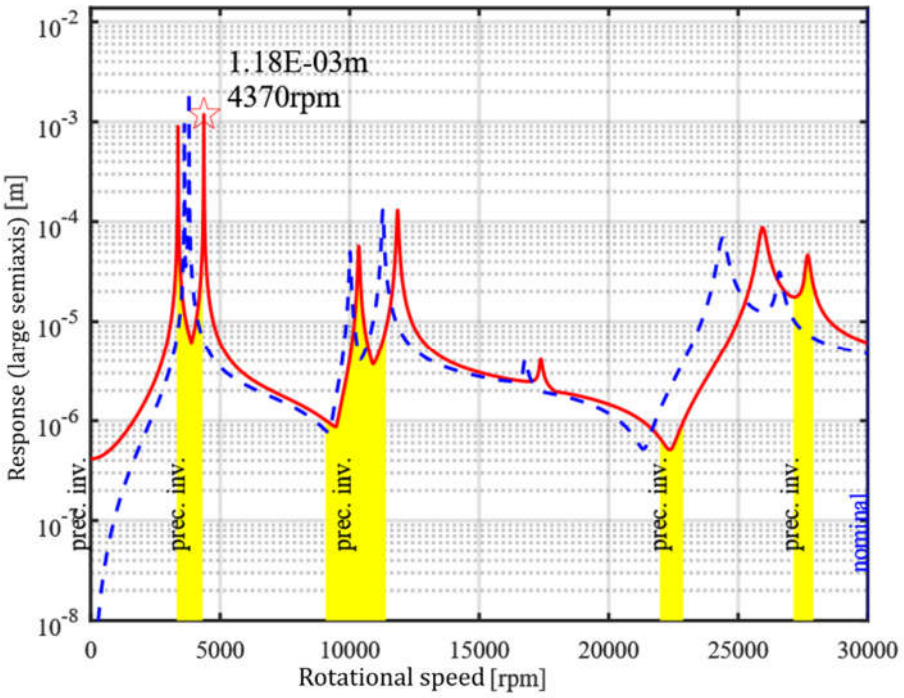

Figure 5.10. Maximum radial displacement of R2 disk due to the imbalance load with the marking of the backward precession domains (prec. inv. yellow band) With blue interrupted line is depicted the inertial case.

5.3.5 Three disks rotor, rotation around the center of mass of the rotor

$\left(\dot{\alpha} = 0rps, \dot{\beta} = 30rps, \dot{\gamma} = 0\right)$

a) Campbell diagram

In this case the axial tension in the shaft due to inertial forces is minimized and thus the expression of the phenomenon of "spin softening" is better highlighted.

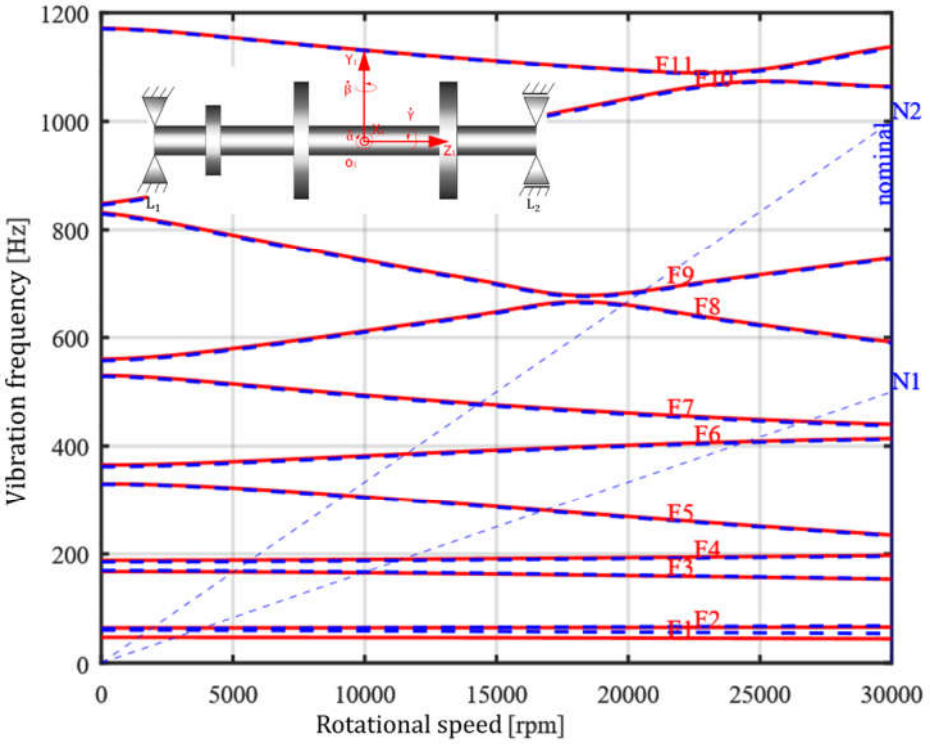

Figure 5.11. Campbell diagram in non-inertial reference system $\left(\dot{\beta} = 30rps\right)$.
With blue interrupted line is depicted the inertial case.

b) Frequency response due to the imbalance load

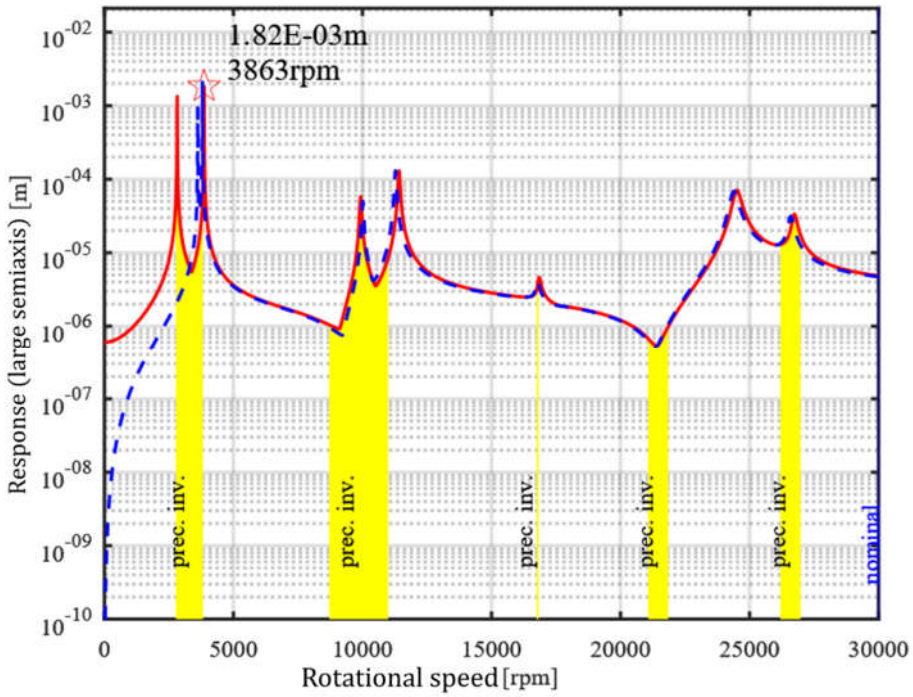

Figure 5.12. Maximum radial displacement of R2 disk due to the imbalance load with the marking of the backward precession domains (prec. inv. yellow band).
With blue interrupted line is depicted the inertial case for comparison.

5.3.6 Three disks rotor, rotation around the shaft opposite end relating to the axial bearing $\left(\dot{\alpha}=0rps,\dot{\beta}=30rps,\dot{\gamma}=0\right)$

a) Campbell diagram

In this case the location of the non-inertial reference system at the opposite end relating the axial bearing causes the compression of the rotor shaft. Thus, the two governing effects, spin softening and shaft compression, combine in an additive manner leading to a decrease in frequencies for all vibration lines and in particular for the F1 vibration line.

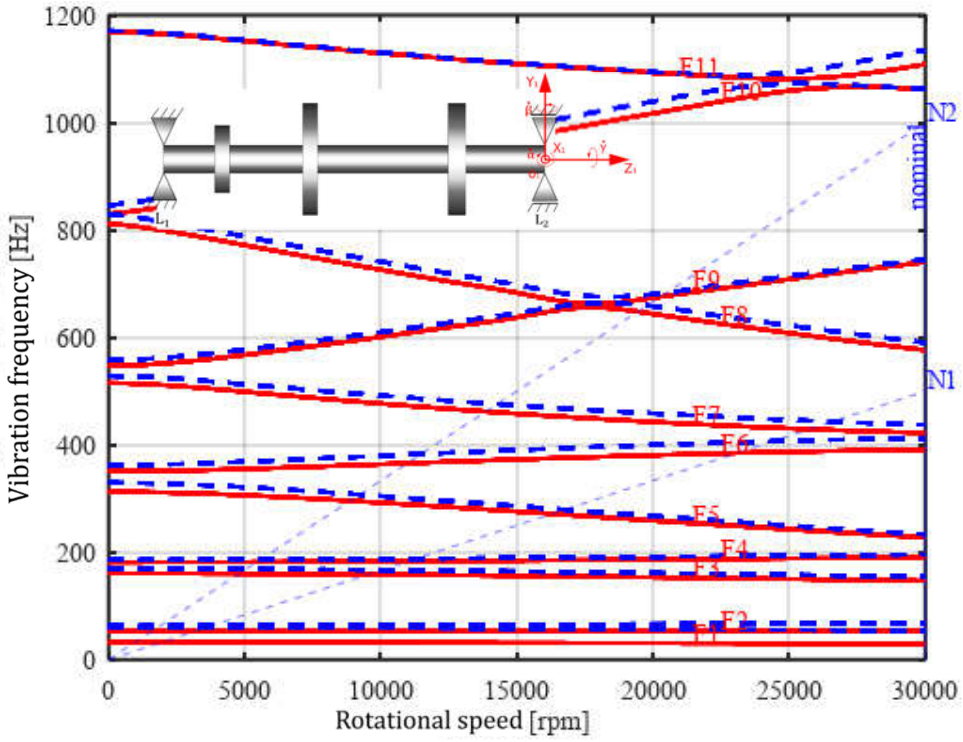

Figure 5.13. Campbell diagram in non-inertial reference system $\left(\dot{\beta}=30rps\right)$. With blue interrupted line is depicted the inertial case.

b) Frequency response due to the imbalance load

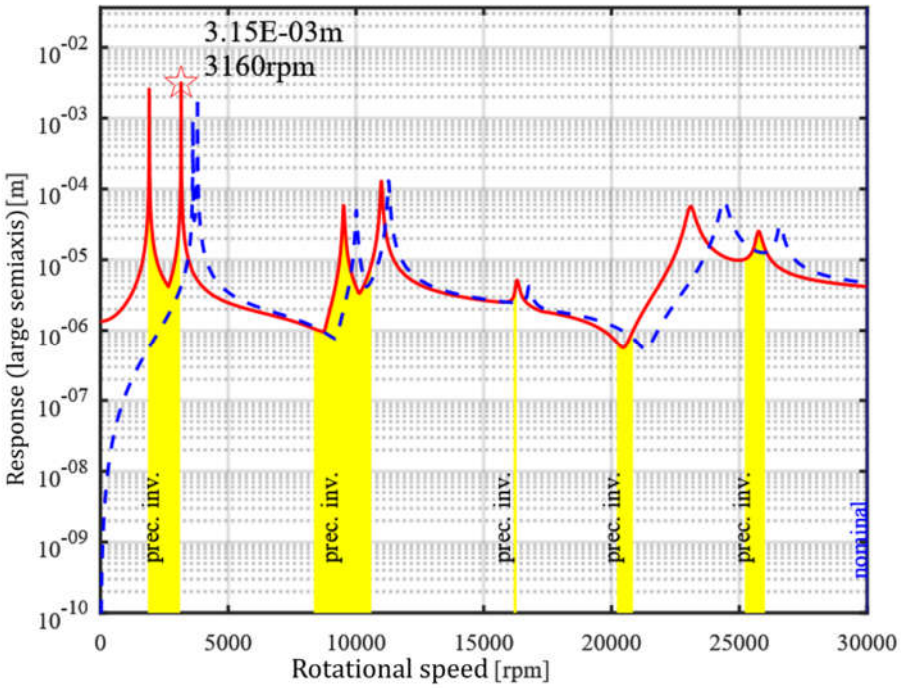

Figure 5.14. Maximum radial displacement of R2 disk due to the imbalance load with the marking of the backward precession domains (prec. inv. yellow band). With blue interrupted line is depicted the inertial case for comparison.

5.4 ROTOR IN NON-INERTIAL REFERENCE SYSTEM SUBJECTED TO ACCELERATIONS DUE TO A ROTATIONAL VECTOR COLLINEAR TO THE BEARING'S AXIS

5.4.1 One disk rotor, direct rotation $\left(\dot{\alpha} = 0rps, \dot{\beta} = 0, \dot{\gamma} = 30rps\right)$

For the rotation of the non-inertial reference system in a direct direction around the bearing axis, the reverse precession movement appears to be faster with the frequency difference corresponding to the rotation around the bearing axis (30rps - »30Hz). On the other hand, the rotation around the bearing axis amplifies the force given by the imbalance and leads to higher radial displacements compared to the inertial case.

a) Campbell diagram

The fundamental frequency shows a noticeable decrease and changes the direction of precession. The other vibration frequencies are larger compared to the inertial case.

b) Frequency response due to the imbalance load

The radial displacement for the first vibration frequency increases greatly. For the other frequencies, the maximum vibration amplitude would be reduced.

5.4.2 One disk rotor, reverse rotation $\left(\dot{\alpha} = 0rps, \dot{\beta} = 0, \dot{\gamma} = -30rps\right)$

In the case of rotation of the non-inertial reference system in the opposite direction relative to the nominal rotor speed, there is a change in the effects of reverse precession and direct precession, which causes the displacement of the F1 and partially F2 + F3 vibration lines by approximately 30Hz. The speed of the non-inertial system $\dot{\gamma}$ is considered constant and therefore it also acts when the speed of the rotary machine Ω is zero, thus generating zero rotational speed precession phenomena.

a) Campbell diagram

The fundamental frequency decreases compared to the inertial case and retains its sense of precession. Due to the gyroscopic moment induced by the rotation of the non-inertial system, the vibration lines in pairs no longer start from the same point (from the same frequency) at zero rotational speed.

b) Frequency response due to the imbalance load

The lateral vibration amplitudes due to the imbalance are smaller than in the inertial case.

5.4.3 Three disks rotor, direct rotation $\left(\dot{\alpha} = 0rps, \dot{\beta} = 0, \dot{\gamma} = 30rps\right)$

For the three disk rotor, the rotation of the non-inertial reference system in the direct direction leads to an increase in the frequencies of the backward precession vibration lines and to a decrease in the frequencies of the direct precession vibration lines. Compared to the inertial case this would lead to the intersection of adjacent vibration lines. In reality this does not happen and a more complex phenomenon takes place. *The vibration lines start as if they are going to intersect but instead of intersecting, the direct precession line turns into a reverse precession line and the reverse precession line turns into a direct precession line.* This can be exemplified for the F5 and F6 vibration lines. It is observed from the Campbell diagram that the F5 line changes between 10000rpm and 12500 rpm speeds from direct precession to reverse precession without intersecting with line F6. Changing the vibration lines is likely to make it impossible to operate in a safety margin of 10% at nominal speed. The lateral displacement under the influence of the imbalance increases compared to the inertial case due to the “spin softening” effect generated by the rotation of the non-inertial system.

a) Campbell diagram

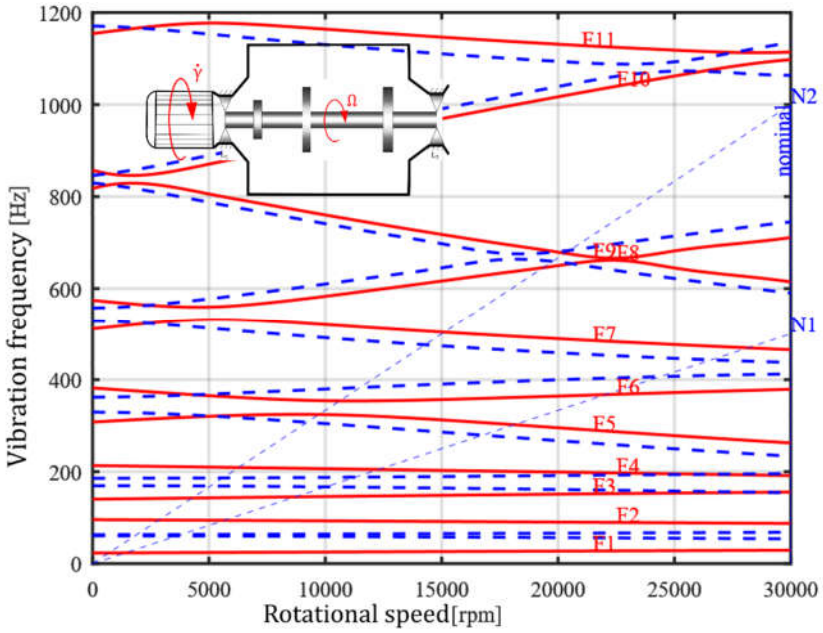

Figure 5.15. Campbell diagram in non-inertial reference system $\left(\dot{\alpha} = 0rps, \dot{\beta} = 0, \dot{\gamma} = 30rps\right)$. With blue interrupted line is depicted the inertial case.

b) Frequency response due to the imbalance load

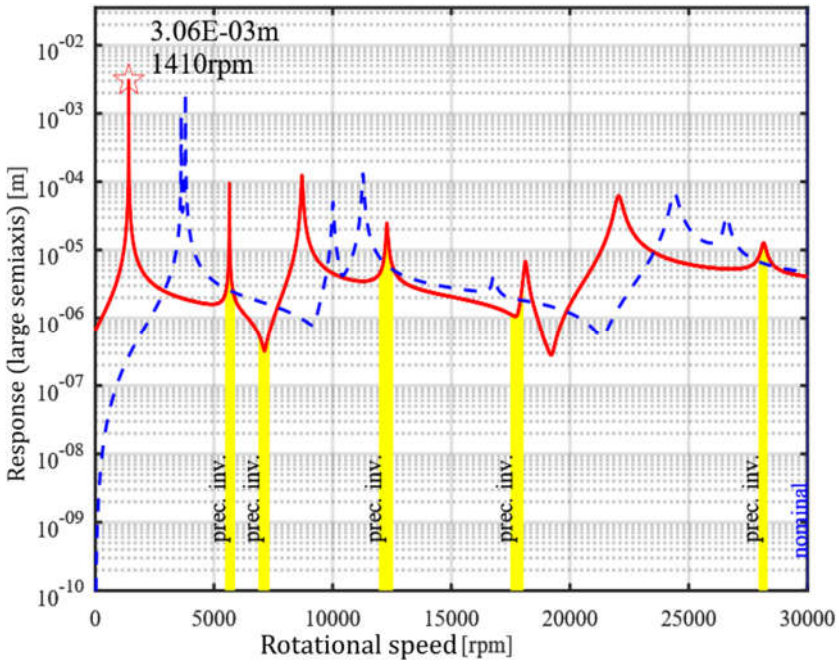

Figure 5.16. Maximum radial displacement of R2 disk due to the imbalance load with the marking of the backward precession domains (prec. inv. yellow band). With blue interrupted line is depicted the inertial case for comparison.

5.4.4 Three disks rotor, reverse rotation $\left(\dot{\alpha}=0rps,\dot{\beta}=0,\dot{\gamma}=-30rps\right)$

For the reverse rotation of the non-inertial reference system Ox1y1z1, the decrease of the vibration frequencies for the reverse precession vibration lines and the increase of the vibration frequencies for the direct precession lines are registered. This is due to the gyroscopic effect of the non-inertial system rotation which has an influence that is added to all speeds. The response due to the imbalance shows a major difference from the inertial case by decreasing the lateral displacement to zero when the rotor speed becomes equal to 30rps (1800rpm). This is explained by the disappearance of the centrifugal force acting on the imbalance. From the point of view of the rotor operation areas, a safety margin of 10% means that the rotor can operate strictly at the nominal speed Nn, the area 81 - 99% being forbidden due to the N1 / F7 intersection.

a) Campbell diagram

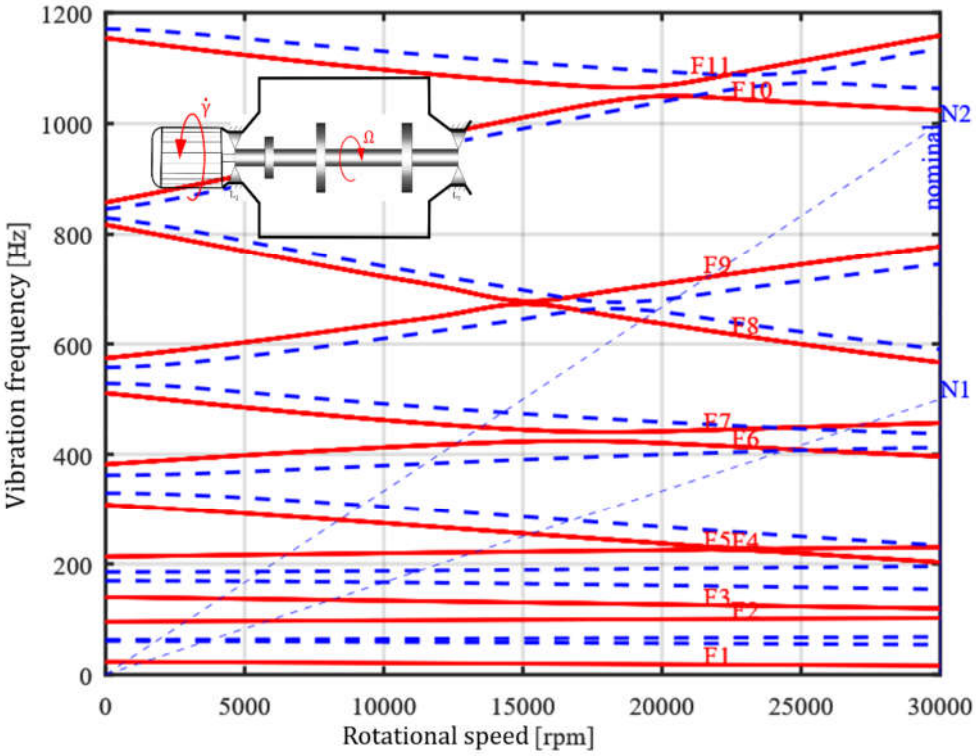

Figure 5.17. Campbell diagram in non-inertial reference system $\left(\dot{\alpha}=0rps,\dot{\beta}=0,\dot{\gamma}=-30rps\right)$. With blue interrupted line is depicted the inertial case for comparison.

b) Frequency response due to the imbalance load

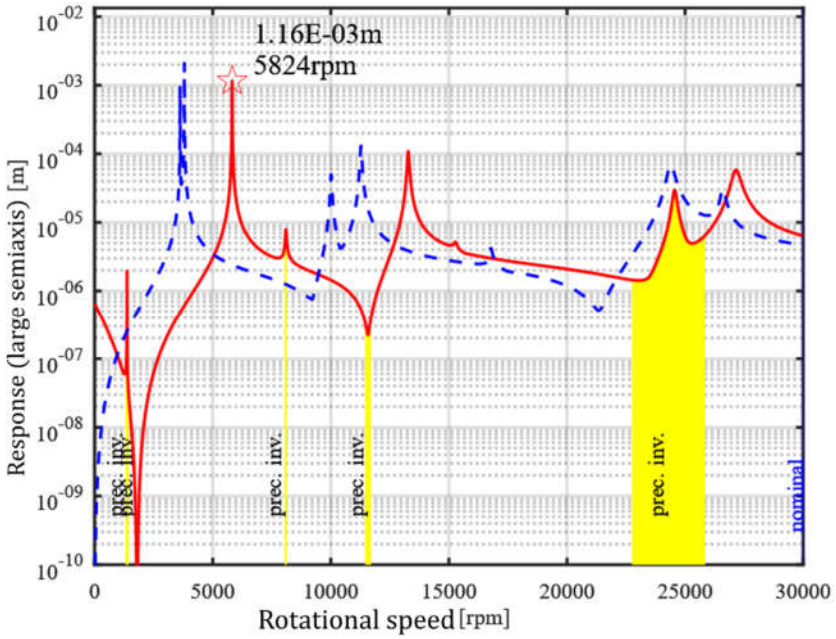

Figure 5.18. Maximum radial displacement of R2 disk due to the imbalance load with the marking of the backward precession domains (prec. inv. yellow band). With blue interrupted line is depicted the inertial case for comparison.

5.5 DETERMINING THE NON-INERTIAL ENVELOPE OF OPERATION FOR THE ROTOR

Two fundamental limits underlie the determination of the non-inertial operating envelope of a rotor in general and these are the maximum allowable Von Mises stress of the materials used and the buckling limit of the rotor shaft. In addition to these two generally valid limitations, other limitations given by operating safety margins, resonances, etc. can be detailed. Below are the non-inertial envelopes for a steel rotor with a yield limit of 2.5E8 Pa. From the first diagram it is observed that when applying axial acceleration, the torque in the rotor must be reduced in order not to exceed the yield limit of the material, the maximum allowable Von Mises stress. The second figure shows the variation of the fundamental vibration frequency in the domain of the operating envelope. In this case, the limitation on the Von Mises stress criterion occurs before the buckling phenomenon occurs so that the latter does not intervene in the construction of the non-inertial envelope.

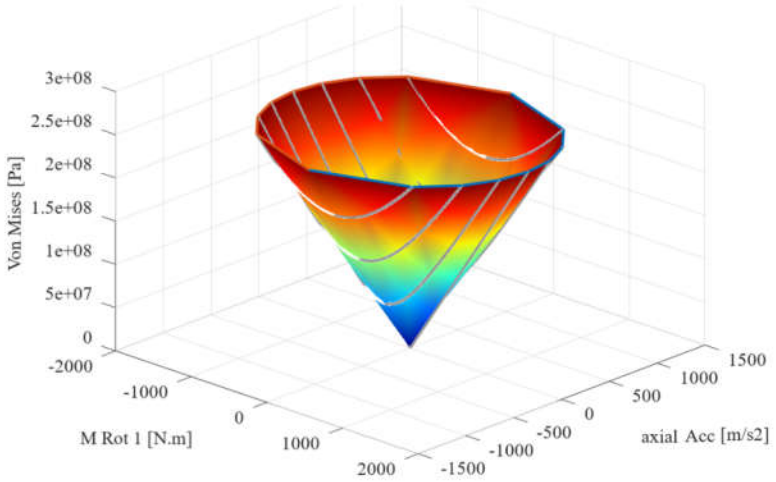

Figure 5.19. The non-inertial operation envelope due to the yield stress of the rotor material.

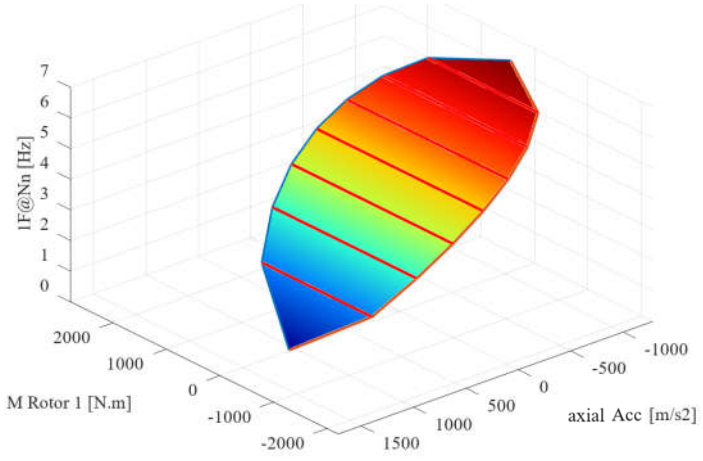

Figure 5.20. Non-inertial operation envelope. Checking the buckling limit due to the fundamental vibration frequency of the rotor.

CONCLUSIONS

C.1. GENERAL CONCLUSIONS

The paper highlights the importance of studying the dynamics of rotors in non-inertial reference systems in the design of rotary machines intended especially for the aerospace field. The approach in the thesis is strongly oriented towards the practical application usually required for the aeronautical engineer and is the result of the challenges encountered by the author during the fifteen years of activity in partnership with renowned companies such as SAFRAN, ESA, AIRBUS, DLR, ONERA , CIAM. Although the examples addressed in the paper are chosen from the literature on the basis of being well known and documented, the way in which the calculation cases are treated are eloquent for all practical cases encountered in the non-inertial field and especially the aerospace field. The worldwide pioneering work of theorists such as Voinea R. and Stroe I. [1] is developed in detail while taking into account current global developments with a focus on the development of finite element techniques [2] capable of analyzing very complex geometric configurations and parts assemblies. The theoretical development was made starting from the simple representation in the form of a material point subjected to various forces often encountered in practical experience such as the presence of axial and radial forces and the torque involved in power transmission between various sections of the rotor. Then, based on the conclusions drawn for the case of the material point, a theory in the field of finite elements was developed. The Timoshenko bar representation was chosen to be enriched with the theoretical elements necessary to perform calculations specific to rotordynamics. The reason is due to the very good accuracy, the relatively high calculation speed and the widespread use with very good results in the field of materials strength calculation and vibration analysis of rotors. Thus, in this thesis, an analysis methodology was developed that meets the requirements of all practical applications of rotors in aerospace. The chapter on numerical applications exemplifies all the typical configurations of non-inertiality that can be encountered in practical work and highlights the importance of considering non-inertial theory in direct comparison with the inertial one commonly used. Depending on the magnitude of the angular velocities involving the non-inertial reference system attached to the rotor as well as the slenderness and other peculiarities of the rotor, one can even reach the situation of catastrophic failure of the rotor. The phenomena involved, related to the buckling of the rotor shaft under the action of accelerations or due to the dramatic change of critical frequencies so as to record overlap over the operating range, were analyzed in detail highlighting the safety measures to be taken for each case.

C.2. ORIGINAL CONTRIBUTIONS

An important contribution of the present thesis is the deduction of the complete form of the Timoshenko theory for bars with the inclusion of the influence of the torsional moment on the lateral vibration frequency. In areas where accurate vibration assessment of

rotating machines such as the aerospace field is required, the Timoshenko bar theory is one of the most widely used because it is generally one of the most advanced theories at present. However for the field of rotors with slender shafts, characterized by the slenderness coefficient of the shaft R / 2L <0.0025 [17] and heavily loaded such as the transmission from the helicopter's anti-torque propeller, the torque that accompanies the power transmission dramatically changes its vibration frequencies . Thus for these cases it is absolutely necessary to consider the influence of the torsional moment on the lateral vibration frequencies. The special utility of this contribution is also given by the much wider field of application which is not limited only to the field of this thesis but affects all rotary machines and especially those with slender shafts.

An additional note of originality is the approach of the theory in the presence of large deformations.

A notable contribution is the elaboration of the numerical program of complex analysis of rotors in non-inertial reference systems, elaborated by the author using the Matlab programming language. [25, 26] With this complex program, all the curves in the thesis were drawn.

The maximum level of simplification of Chapter Five in the field of application can also be considered an important contribution as it makes the non-inertial theory of rotors accessible to most researchers in the field of applied mechanics. The simplification of the presentation was made so as to highlight the phenomena caused by the non-inertial evolution of the rotors not by decreasing the generality of the approach but by judiciously choosing the location of the non-inertial coordinate system in relation to the rotor components and in relation to an inertial system. The direct application in the field of industrial robots is obvious when considering five-axis milling centers in which a robotic arm operates a high speed milling cutter. On the other hand, the construction of robotic arms involves the use of electric motors with relatively high speed whose low torque is transformed by reducing mechanisms into high torque and low angular velocity. It follows that each element of the robotic arms may contain a rotating machine (gearbox wheels) in a non-inertial system. Although not obvious, robotics theory underlies the simplified presentation of Chapter Five on numerical applications. Chasle's theorem [27–29] shows that any motion of a solid body can be considered as a rotation about an axis accompanied by a translation along the same axis. This results in the simplest choice of the non-inertial axis system connected to the rotary machine having the Oz axis coinciding with this axis of motion. However, from a practical point of view, it is more useful to use a non-inertial reference system located on the axis of the rotary machine bearings. The Denavit-Hartenberg [27–29] robotics method is used to transform a non-inertial system moving along an axis (according to Chasle's theorem) into a non-inertial system which rotates along two axes (instead of three for an arbitrary choose non-inertial system) and is collinear with the axis of bearings,.

The merit and contribution of the numerical applications approach is that it provides any aerospace and robotics specialist with a method of qualitatively classifying the effects of a general motion on the rotary machine by interpreting the position of the non-inertial system obtained by the Denavit-Hartenberg method in relation to the center of mass of the rotor and

the axial bearing. For example for a rotor that has the axial bearing positioned to the left of the rotor center of mass and the non-inertial axis system obtained by the Denavit-Hartenberg method is also to the left of the center of mass then the effects of non-inertial rotations will be similar when the non-inertial system is located with origin in the axial bearing.

For the quantitative estimation of these effects the numerical theory developed in the present paper must be applied and depending on the stress limits of the materials and constructive solutions used one can calculate the non-inertial envelope of the rotary machine describing the safe operating range of the rotary machine in a non-inertial system. Since the non-inertial character is given by the three rotational speeds and the six accelerations associated with the axes of the arbitrary chosen non-inertial system, it results that the non-inertial operating envelope is a hypersurface in the nine-dimensional space. For rotors that drive power, respectively torque, it is useful to include it in the inertial envelope to obtain the law of regulation of the rotary machine due to non-inertial loads (rotational speed is adjusted). For the purpose of visualization, diagrams such as those in subchapter 5.5 result, which are very helpful for the preliminary design of both the rotary machine itself and the vehicle that is equipped with this rotary machine. The two universally valid limitations are illustrated, the Von Mises stress limit which cannot exceed the yield limit of the rotor material and the fundamental frequency limit (1F @ Nn) which cannot be zero, in which case the rotor buckling would occur (buckling at compression, torsion or combined).

Last but not least, is to be mentioned the author's contribution in the field of international patents materialized by applying during his doctoral studies for three patents in the field of aviation turbomotors. This was realized through the French patent system in order to increase the safety of air transport for the „fan blade out” (FBO) case. Some of the original contributions mentioned in this paragraphs have been published by the author in national journals, in patent applications in the French patent system as well as at international conferences. [9, 18, 30–39]

This paper introduces in the Romanian literature an updated theory based on the Timoshenko formulation capable of supporting the dynamic analysis for rotors of any degree of complexity, thus constituting an absolutely necessary contribution for the aerospace field.

C.3. PROSPECTS FOR FURTHER DEVELOPMENT

The paper addressed all significant cases for rotors operating in non-inertial reference system. However, a field open to development remains that of the numerical methods used in order to increase the computational speed, especially for non-linear explicit computation. The Runge Kutta method was used in this thesis, a method recognized for its robustness, but which is not satisfactory in terms of computational time. For this purpose, methods based on more efficient algorithms such as Wilson Theta can be developed, methods developed especially for the field of rotordynamics in non-inertial reference system.

Another important direction of development is the analysis of rotary machines with flexible disks. One such case is, for example, high-dilution turbofan rotors, helicopter rotors

or wind turbine rotors. Although there are currently methods to address these issues, the computational speed and the results obtained in order to highlight the phenomena governing rotary machines in a non-inertial reference system can be further improved.

Finally, the finite element method can be refined so that not only the whole rotary machine has a non-inertial reference system but each finite element has its own non-inertial reference system which will be related by a coordinate transformation to the system of non-inertial reference of the rotary machine. This implementation gives full freedom in addressing the large deformations of the rotating machine components regardless of the degree of geometric complexity.

A very difficult problem in the field of dynamics of rotary machines with complex geometry in non-inertial system is the very high computing capacity required to ensure the degree of certainty imposed in practical applications. According to European Space Agency rules, the usual safety factor used in the design and calculation of a spacecraft is 1.25. [40] There are cases where the simplification of geometry by one-dimensional elements such as the Timoshenko type bar does not provide all the information necessary for the validation of the project being necessary also simulations with three-dimensional elements. These are required, for example, for the calculation of stress concentrations at low-radius connections. A computational model with three-dimensional elements such as hexahedrons and tetrahedra will eventually be tens of thousands to millions of times more complex than a simple model with one-dimensional bar-type elements. Consequently, the time and computing infrastructure required will be so large that often this approach is not practically possible given the limited deadlines and the special equipment required on the software and hardware side.

For this purpose, the method of modeling with bar lattice can be developed, it is possible to move very quickly from a one-dimensional model, such as the one treated in the present thesis, to a two-dimensional model in plane and finally to a three-dimensional model. Local refinements can be made to quickly know the behavior of the machine in the critical areas that are most loaded in operation. Another advantage of this technique is the high speed of modeling, calculation and optimization during preliminary design when the emphasis is on validating the solution and less on the accuracy of the results.

Finally, for areas such as aerospace, catastrophic failure scenarios of the various components of the rotary machine can be quickly implemented in order to evaluate and optimize the degree of operational safety. It is known that current standards in aviation require the safe operation of the aircraft even in the event of, for example, the rupture of a turbofan blade. The bar lattice modeling technique is very suitable in these cases because it allows the modeling of cracks, rupture, natively without the need to introduce special elements in the model and without the need to regenerate the stiffness matrix with each change of crack, rupture.

SELECTIVE BIBLIOGRAPHY

[1] Voinea, R., Stroe, I.: Vibrations of rotors situated in non-inertial reference frame. *Mécanique-Matériaux-Electricité, Revue du GAMI,* (446), 1992, p. 58–60.

[2] Vollan, A., Komzsik, L.: *Computational Techniques of Rotor Dynamics with the Finite Element Method*. Boca Raton, FL: CRC Press, 2012.

[3] Jeffcott, H.H.: The lateral vibration of loaded shafts in the neighbourhood of a whirling speed—the effect of want of balance. *Philosophical Magazine Series 6*, **37**, 1919, p. 304.

[4] Kimball, A.L.: Internal friction theory of shaft whirling. *General Electric Review*, **27**, 1924, p. 244–251.

[5] Lomakin, A.A.: Calculation of Critical Speeds and Securing of the Dynamic Stability of Hydraulic High-Pressure Machines with Reference of the Forces Arising in the Gap Seals. *Energomashinotroenie*, **4** (1), 1958.

[6] Alford, J.S.: Protecting turbomachinery from self-excited rotor whirl. *ASME Journal of Engineering for Power*, 1965, p. 333–344.

[7] Stroe, I.: MODELE ŞI SITUAŢII SPECIALE DE FUNCŢIONARE ÎN DINAMICA MAŞINILOR ROTATIVE. *COMOTI*, 1998, p. 8.

[8] Friswell, M.I. et al.: *Dynamics of Rotating Machines*. Cambridge ; New York: Cambridge University Press, 2010.

[9] Stanica, C.M. et al.: Study of Rotating Machineries in A Non-Inertial Reference Frame Subjected to Rotations. *Romanian Journal of Acoustics and Vibration*, **16** (2), 2019, p. 125–136.

[10] Carp-Ciocârdia, D.-C., Stroe, I.: Studii asupra comportării dinamice a unor modele de rotori. *Studii și cercetări de mecanică aplicată*, **53**, 1994, p. 235–241.

[11] Stroe, I., Carp-Ciocârdia, D.-C.: Asupra unor modele pentru studiul vibrațiilor rotorilor. *Studii și cercetări de mecanică aplicată*, **53**, 1994, p. 349–356.

[12] Chen, W.J., Gunter, E.J.: *Introduction to Dynamics of Rotor-Bearing Systems*. Victoria, BC: Trafford Publishing, 2005.

[13] Vance, J. et al.: *Machinery Vibration and Rotordynamics: Vance/Machinery Vibration*. Hoboken, NJ, USA: John Wiley & Sons, Inc., 2010.

[14] Greenhill, A.G.: On the Strength of Shafting When Exposed Both to Torsion and to End Thrust. *Proceedings of the Institution of Mechanical Engineers*, **34** (1), 1883, p. 182–225.

[15] Southwell, R., B. Gough: On the Stability of Rotating Shaft, Subjected Simultaneously to End Thrust and Twist. *British Association for Advancement of Science*, 1921, p. 345.

[16] Golomb, M., Rosemberg, R.: *Critical Speeds of Uniform Shafts Under Axial Torque*. U.S. National Congress for Applied Mechanics. New York, 1961.

[17] Eshleman, R.L., Eubanks, R.A.: On the Critical Speeds of a Continuous Rotor. *J. Eng. Ind*, **91** (4), 1969, p. 1180–1188.

[18] Stanica, C.M. et al.: THE COMPLETE TIMOSHENKO FORM OF TORQUE INFLUENCE ON ROTORS LATERAL VIBRATIONS. *U.P.B. Scientific Bulletin*, **80**, 2018.

[19] Kosmatka, J.B.: An improved two-node finite element for stability and natural frequencies of axial-loaded Timoshenko beams. *Computers and Structures*, **57** (1), 1995, p. 141–149.

[20] Ziegler, H.: *Principles of Structural Stability*. Basel: Birkhäuser, 1980.

[21] Freno, B.A., Cizmas, P.G.A.: A computationally efficient non-linear beam model. *International Journal of Non-Linear Mechanics*, **46** (6), 2011, p. 854–869.

[22] Narayan Rao, J.S.: *History of rotating machinery dynamics*. Dordrecht: Springer, 2011.

[23] Software, M.: *Advanced Dynamic Analysis User's Guide*. MSC. Software, 2017.

[24] Lalanne, M., Ferraris, G.: *Rotor dynamics prediction in engineering*. Chichester (UK): John Wiley and Sons, 1998.

[25] Natick: *MATLAB*. The MathWorks Inc., 2018.

[26] Eaton, J.W. et al.: *GNU Octave*. 2019.

[27] Featherstone, R.: *Robot Dynamics Algorithms*. New York: Springer Science+Business Media, LLC., 1987.

[28] Lung-When, T.: *Robot Analysis: The Mechanics of Serial and Parallel Manipulators*. John Wiley & Sons, Inc., 1999.

[29] Marghitu, D.B.: *Mechanisms and Robots Analysis with Matlab*. Auburn, USA: Springer - Verlag London Limited, 2009.

[30] Meillard, L., Stanica, C.M., et al.: *Design of a counter rotating fan using a multidisciplinary and multifidelity optimisation under high level of restrictions*. International Society for Air Breathing Engines. Manchester, United Kingdom., 2017.

[31] Stanica, C.M., Stroe, I.: Vibration of rotor blades with large deformations in a rotating noninertial reference frame. *U.P.B. Scientific Bulletin, Series D*, **80** (2), 2018.

[32] Mihalache, R., Stanica, C.M., et al.: *Manufacturing a composite structure with applications in aeronautical field that can absorb displacements on different directions*. Venice, Italy, 2011.

[33] Mihalache, R., Stanica, C.M., et al.: Advanced Strategic Planning and Capability Identification in order to develop a Liquid Hydrogen Turbopump. *Applied Mechanics and Materials*, **555**, 2014, p. 66–71.

[34] Grodent, C., Stanica, C.M., et al.: *Wide Range Thermal Test Facility For JUICE Large Appendages*. 14th European Conference on Spacecraft Structures, Materials and Environmental Testing. Toulouse, France: ECSSMET, 2016.

[35] Grodent, C., Stanica, C.M., et al.: *Wide Range Thermal Test Facility For JUICE Large Appendages, Design and Results*. 6th International Workshop on Verification and Testing of Space Systems. Torino ,Italy, 2019.

[36] Stanica, C.M. et al.: *(Aplicatie Patent WO2019038500-A1) Method for manufacturing outward guiding aerofoil blade of turbomachine, involves forming intersection between first fibrous wall preform and second fibrous wall preform so as to form leading edge or trailing edge of blade*. 2019.

[37] Stanica, C.M. et al.: *(Aplicatie Patent FR3070421A1) Pale pour turbomachine et son procede de fabrication*. 2019.

[38] Stanica, C.M. et al.: *(Aplicatie Patent FR3070427-A1) Insert pour la fixation d'un composant sur un support de turbomachine (1)*. 2019.

[39] Stanica, C.M. et al.: *(Aplicatie Patent FR3070428-A1) Insert pour la fixation d'un composant sur un support de turbomachine (2)*. 2019.

[40] European Space Agency: *Space engineering. Structural factors of safety for spaceflight hardware.* ECSS Secretariat ESA-ESTEC Requirements & Standards Division, 2009.